UNITED NATIONS UNIVERSITY
GEOTHERMAL TRAINING PROGRAMME
Orkustofnun, Grensasvegur 9,
IS-108 Reykjavik, Iceland

Reports 2011
Number 9

JOINT 1D INVERSION OF TEM AND MT RESISTIVITY DATA WITH AN EXAMPLE FROM THE AREA AROUND THE EYJAFJALLAJÖKULL GLACIER, S-ICELAND

Alae-Eddine Barkaoui
Laboratory of Mineral Deposit, Hydrogeology & Environment
University Mohamed I^{st,}
Oujda
MOROCCO
barkalae@yahoo.fr

ABSTRACT

Due to the recent eruptive events in Eyjafjallajökull, many projects have been started, collecting more information to gain a deeper understanding about volcanic structures and processes. This can help to better predict the nature and timing of volcanic threats. Glacier covered volcanoes are of special interest since these are phreato-magmatic and capable of producing sudden glacial floods.

In order to investigate the resistivity structure beneath and around Eyjafjallajökull glacier, the Dublin Institute for Advanced Studies (DIAS) and Iceland GeoSurvey (ISOR) carried out the first step of an MT survey in 2011 including 26 pairs of MT and TEM soundings around the volcano, where each MT sounding took 2 days to record. The MT (Magnetotelluric) and TEM (Transient Electro Magnetic) methods are far more sensitive to fluid distribution (in this case partial melt) than any other geophysical method, thus leading to this pilot study. TEM soundings were carried out at the same locations as the MT soundings in order to correct for static shifts. A remote reference MT station was running simultaneously at several tens of kilometres distance to allow the state-of-the-art remote-referencing technique to improve the signal to noise ratio. Joint 1D (one-dimensional) inversion of magnetotelluric (MT) and central loop transient electromagnetic (TEM) data was done by fitting both data sets using the same 1D resistivity model.

1. INTRODUCTION

Before drilling operations commence for the exploitation of a geothermal resource, prefeasibility investigations using geological, geochemical and geophysical methods need to be carried out in order to gain a better understanding of the subsurface geological and tectonic configuration of the region under study. In fact, geophysical exploration enables one to unravel the tectonic features and associated thermal regimes that host geothermal reservoirs. Since drilling geothermal wells is expensive, using geophysical methods can bring down the cost to a certain degree. This is true in any underground exploration or investigation for groundwater, mineral resources, mining activity, etc. (Chandrasekharam and Bundschuh, 2008).

Surface geophysical exploration methods help indirectly in obtaining the physical parameters of geothermal systems. Electrical, magnetic, seismic, thermal and gravity surveys are a few of the methods commonly employed for geothermal exploration. All these investigations are carried out on the surface over the geothermal regions. The effectiveness of these geophysical methods was greatly increased when emphasis was shifted from prospecting the geology and the structures that contain the geothermal fluids to prospecting the fluids themselves and concentrating on determining the parameters which are most sensitive to changes in temperature (Hersir and Björnsson, 1991). The point of these geophysical methods is to measure some physical properties related to the geothermal system: temperature (°C), electrical resistivity (Ωm), magnetization (A/m), density (g/cm^3), elasticity (N/m^2), and seismic velocity (m/s).

In this report, the focus will be on two of the most important electromagnetic resistivity methods in geothermal prospection:

- The Transient Electromagnetic Method (TEM), and
- The Magnetotelluric method (MT).

1D modelling of MT and TEM soundings from an area around the Eyjafjallajökull glacier in S-Iceland was carried out and the results are represented as resistivity maps and cross-sections. The processed data are published separately as a special appendices report (Barkaoui, 2011).

2. ELECTROMAGNETIC RESISTIVITY METHODS IN GEOTHERMAL EXPLORATION

Measuring the electrical resistivity of the subsurface is the most powerful prospecting method in geothermal exploration (Hersir and Björnsson, 1991). Resistivity is directly related to the properties of interest like salinity, temperature, porosity (permeability) and alteration. To a great extent, these parameters characterize the reservoir.

The specific resistivity, ρ, is defined through Ohm's law. The electrical field strength, $\boldsymbol{E}$ (V/m) at some point in a material is proportional to the current density, $\boldsymbol{j}$ (A/m^2):

$$E = \rho j \tag{1}$$

The proportional constant, ρ, depends on the material and is called the (specific) resistivity, measured in Ωm. The reciprocal value of resistivity is conductivity ($1/\rho = \sigma$).

Resistivity can also be defined as the ratio of the potential difference, ΔV (V/m), to the current, I (A), across material which has a cross-sectional area of 1 m^2 and is 1 m long:

$$\rho = \frac{\Delta V}{I} \tag{2}$$

Electrical conductivity in minerals and solutions takes place by the movement of electrons and ions. Most rocks near the earth's surface have low conductivity. Conduction of electricity is mostly through groundwater contained in pores in the rocks and along surface layers at the contact of rocks and solutions.

The common principle of all resistivity sounding methods is to induce an electrical current into the earth and monitor signals, normally at the surface, generated by the current distribution (Hersir and Björnsson, 1991). Direct current soundings, such as Schlumberger soundings, are done by injecting a current into the ground through electrodes at the surface; then the signal measured is the electric field

(the potential difference over a short distance) generated at the surface. In magnetotellurics (MT), the current in the ground is induced by time variations in the earth's magnetic field, and the signal measured is the electric field at the surface. MT is a passive method; the signal source is not man-made. In transient electromagnetics (TEM), the current is also induced by a time-varying magnetic field but, in this case, the current source is not a natural field, rather the source is of a controlled magnitude generated by current in a loop or a grounded dipole and the monitored signal is the decaying magnetic field at the surface. TEM is an active method; the signal source is man-made – it is artificial.

2.1 Factors affecting electrical resistivity

2.1.1 Salinity of water

The bulk resistivity of a rock is to a large extent controlled by the resistivity of the pore fluid which is dependent on the salinity of the fluid. An increase in the total amount of dissolved ions can increase the conductivity by large amounts (Figure 1). The conductivity of a solution depends on mobility and the concentration of the ions. This is given by the equation (Hersir and Björnsson, 1991):

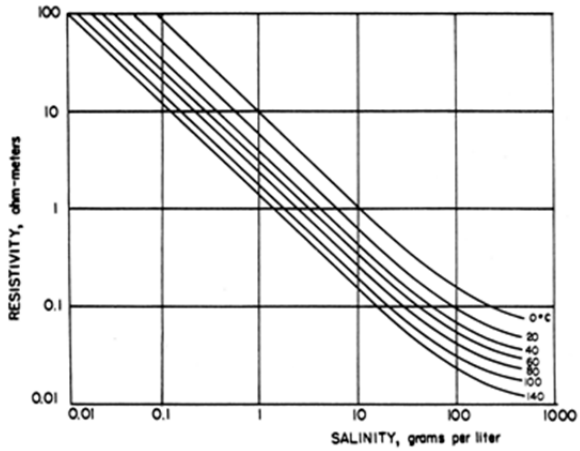

FIGURE 1: The resistivity of solutions of sodium chloride as a function of concentration and temperature (Keller and Frischknecht, 1966)

$$\sigma = {}^{1}/_{\rho} = F(c_1\, q_1 m_1 \; + \; c_2\, q_2 m_2 + \; \ldots\ldots) \tag{3}$$

where σ = Conductivity (S/m);
F = Faraday's number (96,500 C);
c_i = Concentration of ions;
q_i = Valence of ions;
m_i = Mobility of different ions.

An increase in the water content and an increase in the total amount of dissolved solids are frequently associated with geothermal activity.

2.1.2 Porosity

Porosity (φ_t) is the ratio between pore volume (V_v) and the total volume of a material (V_T). This is given by the ratio:

$$\varphi_t = \frac{V_v}{V_T} \tag{4}$$

The resistivity of water-saturated rocks often varies approximately as the inverse power of the porosity according to an empirical formula given by Archie (1942):

$$\rho = \rho_w a {\varphi_t}^{-n} \tag{5}$$

where ρ = Bulk (measured) resistivity (Ωm);
ρ_w = Resistivity of the pore fluid (Ωm);
φ_t = Porosity;
$a,\ n$ = Empirical constants;

Archie´s law can also be written as:

$$\rho = F\,\rho_w \tag{6}$$

where F $= a\varphi_t^{-n}$ = Formation factor.

In some rocks, part of the pore space may be occupied by air (above the water table) or by natural gas, carbon dioxide or petroleum, all of which are insulators. In such cases, Archie's law is modified as follows (Zhdanov and Keller, 1994):

$$\rho = \rho_w a\varphi_t^{-n} f^c \tag{7}$$

Experiments show that Archie's law is only valid for conductive solutions, with $\rho_w \leq 2$ Ωm (Flóvenz et al., 1985).

Permeability is the capacity of a porous material for transmitting a fluid; it is expressed as the amount of fluid of specified viscosity, under the influence of a given pressure that passes through a sample having a certain cross-section and thickness. Permeability is largely dependent on the size and shape of the pores in the substance and, in granular materials such as sedimentary rocks, by the size, shape, and packing arrangement of the grains. The permeability of a rock is given by the following equation:

$$K = \frac{Q\eta L}{AP} \tag{1}$$

where K = Permeability (m^2);
Q = Fluid flowrate (m^3/s);
η = Fluid viscosity (kg/ms);
L = Length of the rock (m);
A = Cross-sectional area available for flow (m^2); and
P = Pressure drop (Pa).

2.1.3 Temperature

At moderate temperatures, 0-200°C, the resistivity of aqueous solutions decreases with increasing temperature (Figures 1 and 2). This is due to an increase in ion mobility caused by a decrease in the viscosity of the water. Dakhnov (1962) has described this relationship:

$$\rho_w = \frac{\rho_{wo}}{1 + \alpha(T - T_o)} \tag{9}$$

where ρ_w = Resistivity of the fluid at temperature T (Ωm);
ρ_{wo} = Resistivity of the fluid at temperature T_0 (Ωm);
α = Temperature coefficient of resistivity ($°C^{-1}$);
T_0 = Reference temperature (°C).

At high temperatures, a decrease in the dielectric permittivity of the water results in a decrease in the number of dissociated ions in solution. Above 300°C, fluid resistivity starts to increase (Quist and Marshall, 1968).

2.1.4 Water-rock interaction and interface conduction

The alteration process and the resulting type of alteration minerals are dependent on the type of primary minerals, the chemical composition of the geothermal fluid and temperature. The intensity of the alteration is, furthermore, dependent on temperature, time and the texture of the host rocks.

Alteration intensity is normally low for temperatures below 50°C (Figure 3). At temperatures from 100 to 220°C, low-temperature zeolites and clay mineral smectite are formed. Smectite has hydrated and loosely bound cations between the silica plates, making the mineral conductive and with a high cation exchange capacity (Árnason et al., 2000). In the temperature range from 220 to about 240°C, the zeolites disappear and the smectite is transformed into chlorite in a transition zone, the so-called mixed-layered clay zone, where smectite and chlorite co-exist in a mixture. At about 240°C, smectite disappears and chlorite is the dominant mineral, marking the beginning of the chlorite zone with increased resistivity, since chlorite minerals have cations that are fixed in a crystal lattice, making the mineral resistive. At still higher temperatures, above 240°C, epidote becomes abundant in the so-called chlorite-epidote zone (Árnason et al., 2000).

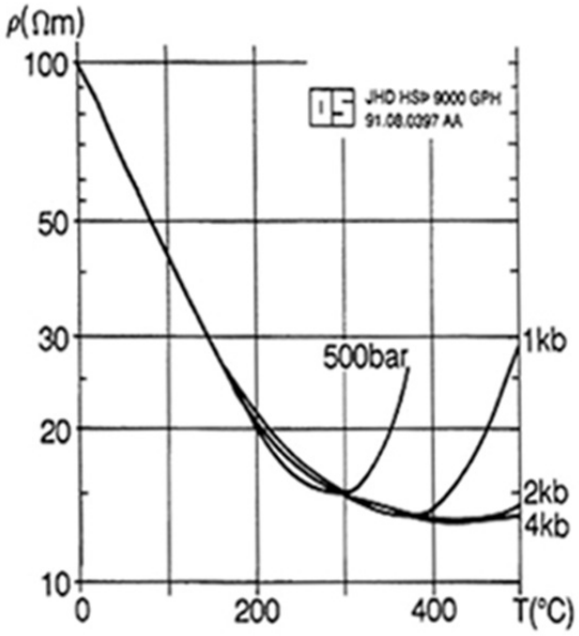

FIGURE 2: Electrical resistivity as a function of temperature at different pressures (Hersir and Björnsson, 1991; modified from Quist and Marshall, 1968)

Normally one would expect the resistivity of a geothermal system to decrease with increasing temperature. However, in high-temperature volcanic areas the resistivity in the chlorite and chlorite-epidote alteration zone increases, due to an extremely low concentration of mobile cations. Figure 4 demonstrates the relationships between resistivity, alteration and temperature both for saline and fresh water systems. At depths, where resistivity increases below a low-resistivity zone, a chlorite alteration zone is expected, indicating a temperature of 250°C or higher, provided the alteration is in equilibrium with the temperature. If the geothermal system has cooled down, then the alteration remains the same and the resistivity structure is the same. In such a case, the interpretation of the resistivity structure can be misleading since it reflects alteration minerals that were formed in the past (Hersir and Árnason, 2009).

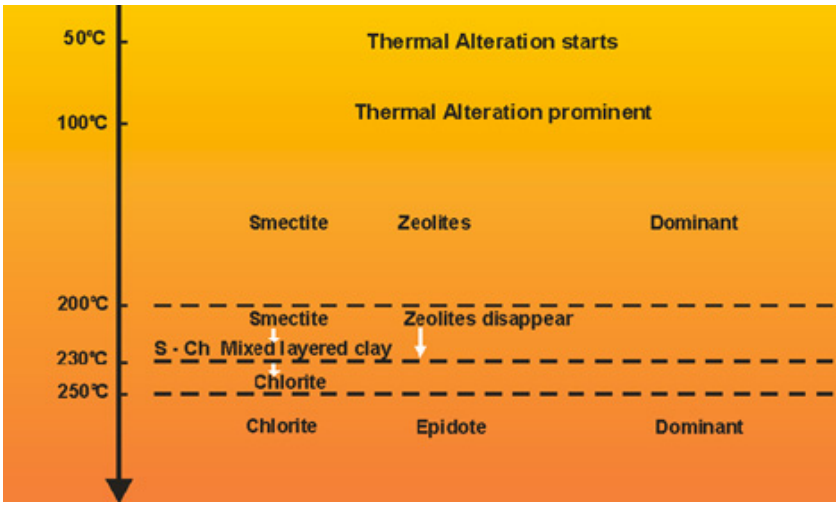

FIGURE 3: Alteration mineralogy and temperature (taken from Hersir and Árnason, 2009)

2.2 Electrical methods

Electrical methods employ a variety of measurements of the effects of electrical current flow within the earth. The phenomena that can be measured include current flow, electrical potential (voltage), and electromagnetic fields. Electrical methods can be divided into the following categories and subcategories (Hersir and Björnsson, 1991):

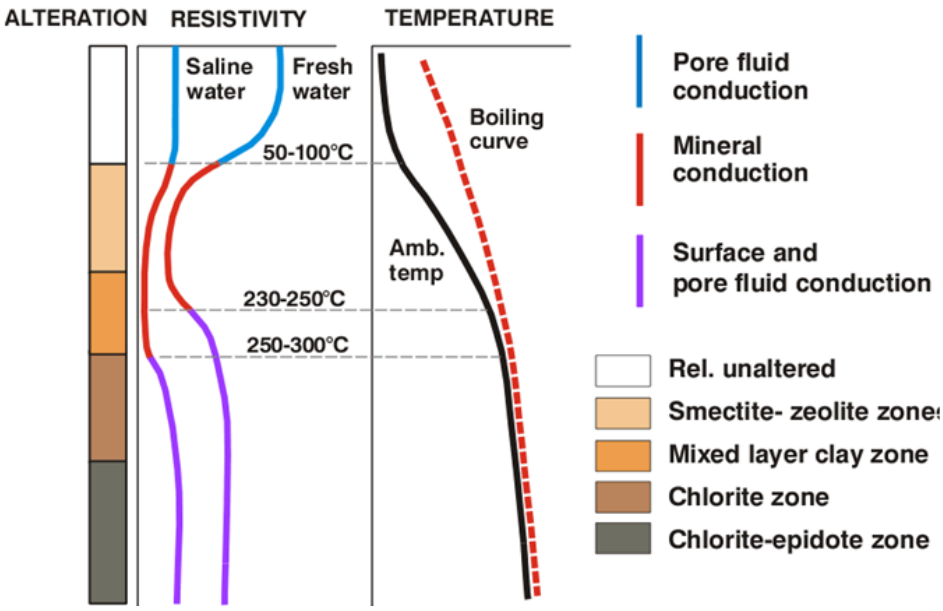

FIGURE 4: The general resistivity structure of the basaltic crust in Iceland summarized (taken from Flóvenz et al., 2005)

DC methods

This is an active method that employs the measurement of electrical potential associated with subsurface electrical current flow generated by a DC, or slowly varying AC source. Two main types of measurements can be distinguished, and a third mentioned:

- Resistivity sounding. Measurements are made at a specified fixed central point for different distances between the electrodes. It is used to measure variations in resistivity with depth. Example: Schlumberger soundings, here the potential electrodes remain "fixed" and the current electrodes are expanded along a symmetrical line from the centre of the profile.
- Resistivity profiling. Electrode arrangement with fixed distances is used and measurements are made as the entire array is moved along a profile. It is designed to locate lateral variations in resistivity. Example: Head-on profiling.
- Self potential (SP). This is a passive method that employs measurements of naturally occurring electrical potentials.

Electromagnetic (EM) methods

Electromagnetic methods in geophysics have been developed since the 1950s by Cagniard (1953) and Tikhonov (1950) based on Maxwell's equations that are composed of Ampere's Law, Gauss's and Faraday's law (Equations 12-15) as expressed by Jones et al. (1989), Vozoff (1991), and Zhdanov and Keller (1994). The equations describe the magnetic and electric fields and their relationship. The strength of the electromagnetic fields varies from one body to another depending on the petrophysical properties of the body and other factors. The essential physical properties of electromagnetic fields are electrical resistivity or conductivity, magnetic permeability and electric permittivity. The physical properties link the electromagnetic induction to the transmitter and the receiver. The counteraction of electric and magnetic fields causes electromagnetic fields to travel and diffuse from the air to the subsurface. The physical properties of rocks govern the propagation and the depth of penetration of the electromagnetic waves in the subsurface. The electromagnetic induction processes require a primary wave source (transmitter) and a conductor. We distinguish between:

- Time domain or transient electromagnetic method (TEM): A magnetic field is built up by transmitting a constant current into a loop or grounded dipole, the current is turned off and the transient decay of the magnetic field is measured.

- Magnetotellurics (MT) and audio-magnetotellurics (AMT): The fluctuations in the natural magnetic field of the earth and the induced electric field are measured. Their ratio is used to determine the apparent resistivity.

The central-loop TEM sounding method has several advantages over conventional DC sounding methods (Árnason, 1989). The transmitter couples inductively to the earth and no current has to be injected into the ground. This is of great importance in areas where the surface is highly resistive (Árnason, 1989). In Schlumberger soundings, the monitored signal is low when surveying over low-resistivity structures like a geothermal area, whereas in TEM soundings it is relatively strong (Árnason, 1989). Secondly, the fact that the monitored signal is a decaying magnetic field, rather than an electric field at the surface, makes the results much less dependent on local resistivity conditions at the receiver site (Sternberg et al., 1988). Distortions due to local resistivity inhomogeneities at the receiver site can be a severe problem in DC soundings as well as in MT soundings (Árnason, 1984; 2008). Thirdly, central-loop TEM is less sensitive to lateral resistivity variations than DC methods. TEM soundings are much more downward-focused than DC soundings. One-dimensional inversion is better justified in the interpretation of central-loop TEM soundings than in DC soundings

Electromagnetic techniques have proven to be among the most useful geophysical methods for the investigation of geothermal regions. This is due to the fact that the spatial distribution of conductivity in a geothermal area is not only determined by the host rock distribution, but is directly related to the distribution of the actual exploration target - hot water (Berktold, 1983).

2.3 The central-loop transient electromagnetic method (TEM)

In the central-loop TEM sounding method, a loop of wire is placed on the ground and a constant magnetic field of known strength is built up by transmitting a constant current into the loop (Figure 5).

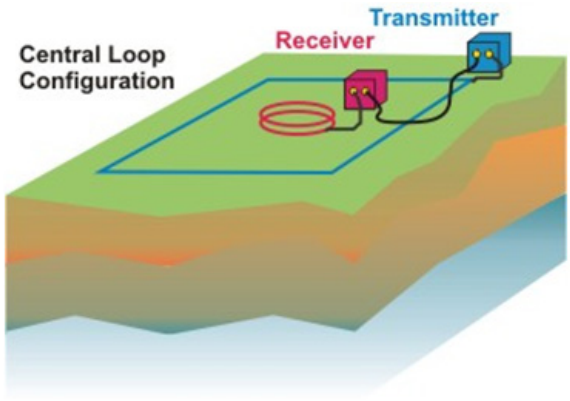

FIGURE 5: The configuration in the central-loop TEM method (modified from Nabighian and MacNae, 1988)

The principles of TEM (Time-Domain Electromagnetic Methods) resistivity sounding are relatively easily understood. The process of abruptly reducing the transmitter current to zero induces, in accordance with Faraday's law, a short-duration voltage pulse in the ground, which causes a loop of current to flow in the immediate vicinity of the transmitter wire. In fact, immediately after the transmitter's current is turned off, the current loop can be thought of as an image in the ground of the transmitter loop (Figure 6). However, due to finite ground resistivity, the amplitude of the current starts to decay immediately. This decaying current similarly induces a voltage pulse that causes more current to flow, but now at a larger distance from the transmitter loop, and also at greater depth, as shown in Figure 7. This deeper current flow also decays due to the finite resistivity of the ground, inducing even deeper current flow and so on.

The depth of penetration in the central loop TEM-sounding is dependent on how long the induction in the receiver coil can be traced before it is drowned in noise. At so-called late times, the induced voltage in the receiving coil in a homogeneous half space of conductivity, σ is (Árnason, 1989):

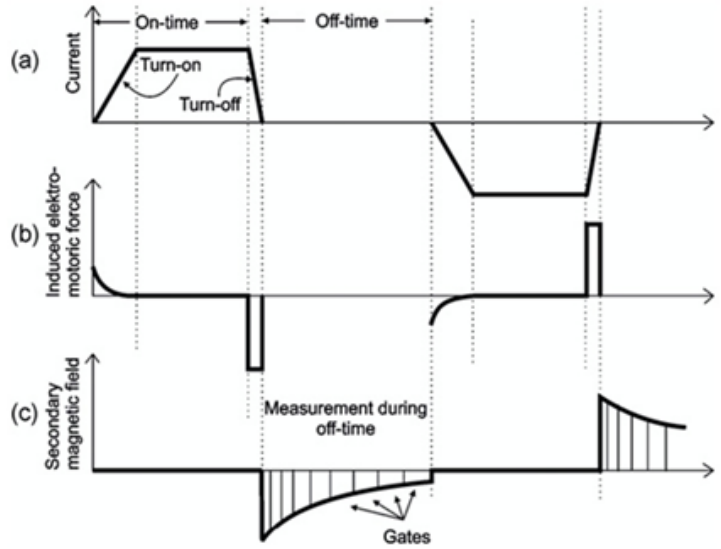

FIGURE 6: Basic principles of the TEM method: (a) The current flow in the transmitter loop; (b) The induced electromotive force in the ground; and (c) The secondary magnetic field measured at gates after the current is turned off in the receiver coil (from Christensen et al., 2006)

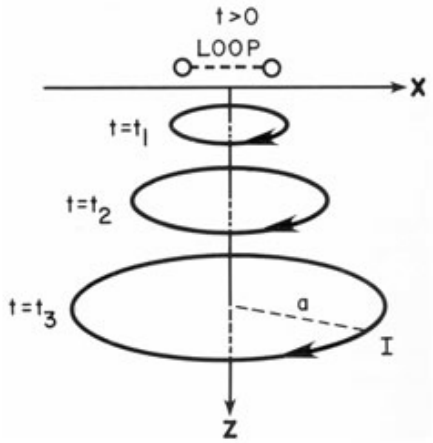

FIGURE 7: Propagation of currents in the underground (Nabighian and MacNae, 1991)

$$V(t,r) \approx I_0 \frac{C(\mu_0 \sigma r^2)^{\frac{3}{2}}}{10\pi^{\frac{1}{2}} t^{\frac{5}{2}}} \qquad (10)$$
$$where \quad C = A_r n_r A_s n_s \frac{\mu_0}{2\pi r^3}$$

and t = Time elapsed after the transmitter current is turned off (s);
A_r = Cross-sectional area of the receiver loop (m^2);
A_s = Cross-sectional area of the transmitter loop (m^2);
n_r = Number of windings in the receiver loop;
n_s = Number of windings in the transmitter loop;
μ_0 = Magnetic permeability (H/m);
I_0 = Current in the transmitter loop (A);
r = Radius of the transmitter loop (m);
$V(t,r)$ = Transient voltage (V).

This shows that the transient voltage for late times, after the current in the transmitter loop is abruptly turned off, is proportional to $\sigma^{3/2}$ and falls off with time as $t^{-5/2}$. This leads to the definition of the late time apparent resistivity by solving for the resistivity in Equation 10, leading to Equation 11:

$$\rho_a = \frac{\mu_0}{4\pi}\left[\frac{2I_0\mu_0 A_r\eta_r A_s\eta_s}{5t^{5/2}\, V(t,r)}\right]^{2/3} \qquad (11)$$

Homogeneous earth

The time-behaviour of the diffusing current is divided into three phases according to their characteristics, as illustrated in Figure 8, which shows induced voltage as a function of time for a homogeneous earth. In the early phase the induced voltage is constant in time. In the intermediate phase, the voltage starts to decrease with time and with steadily increasing negative slope on a log-log scale until the late time phase is reached where the voltage response decreases with time in such a way

that the logarithm of the induced voltage decreases linearly as a function of the logarithm of time. The slope of the response curve in the late phase is -5/2, in accordance with Equation 10 which is only valid for the late-time phase.

Figure 9 shows that the apparent resistivity at early time increases with decreasing resistivity of the half space and also that the transitions from early to late time get shifted towards earlier times as the resistivity of the half space increases. However, it should be noted that the response curve has the same shape for the different half space resistivities. When the apparent resistivity for a homogenous half-space is plotted as a function of time, it approaches asymptotically the true resistivity of the half- space for late times, as can be seen in Figure 9.

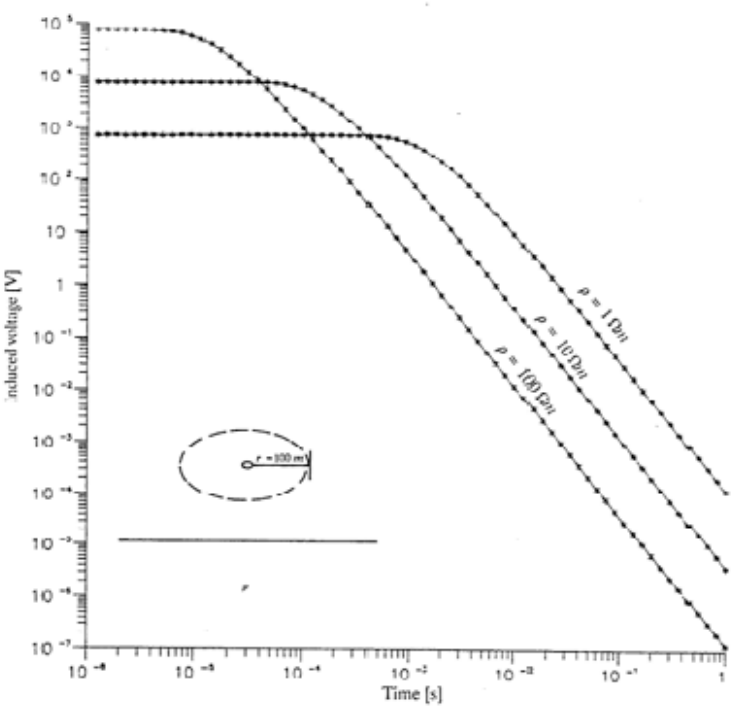

FIGURE 8: Voltage response for homogeneous half space of 1, 10, and 100 Ωm (from Árnason, 1989)

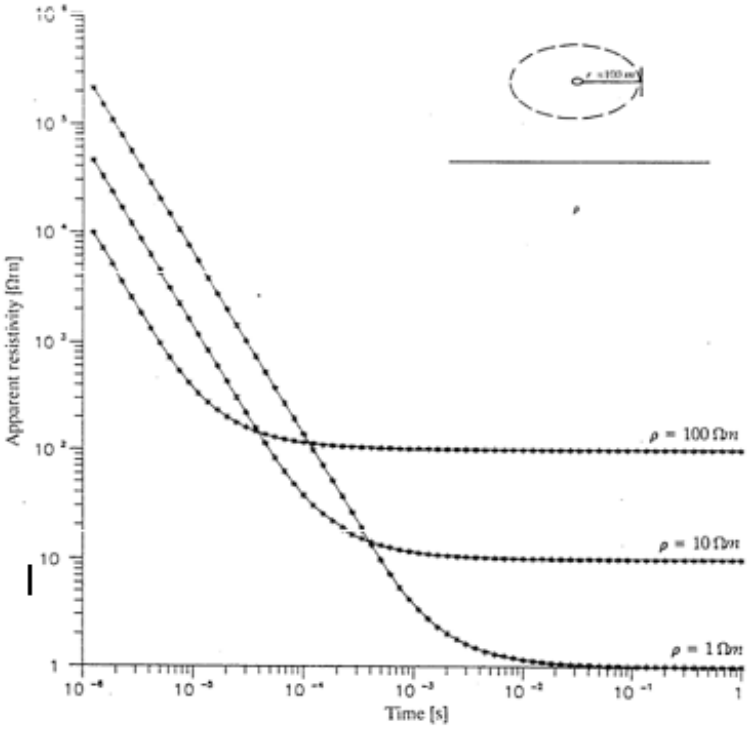

FIGURE 9: Late time apparent resistivity for homogeneous half space of 1, 10 and 100 Ωm (from Árnason, 1989)

2.4 The magnetotelluric (MT) resistivity method

The magnetotelluric (MT) method is a passive electromagnetic geophysical method used to image the earth's subsurface resistivity structure. Natural variations in the earth's magnetic field induce electric currents (or telluric currents) in the ground, which depend on the earth's resistivity. Both magnetic and electric fields are measured on the earth's surface in two orthogonal directions (Figure 10).

The ratio of the orthogonal electric field and the magnetic field, the impedance tensor holds information about subsurface conductivity. The high frequency gives information about the resistivity at shallow depths while the low frequency provides information about the deeper laying structures. At frequencies higher than 1 Hz, the magnetic source originates from lightning discharges in the equatorial belt while the low frequencies, < 1 Hz, originate from the interaction between solar wind

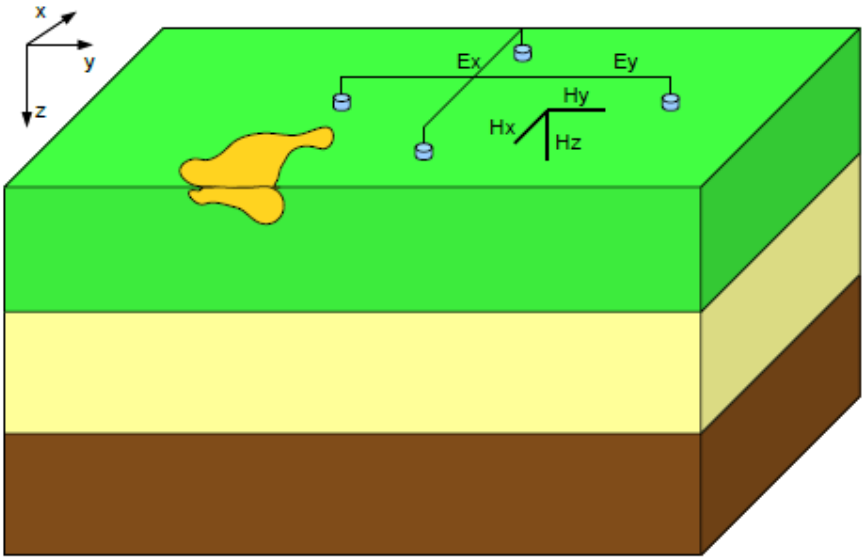

FIGURE 10: MT setup in an internal coordinate system. The setup measures the electrical field in an orthogonal horizontal direction and magnetic field in orthogonal vertical and horizontal directions (Rosenkjær, 2011)

and the earth's magnetic field. These natural phenomena create the MT source signals over the entire frequency spectrum, generally 10 kHz to a period of a few thousand seconds.

The MT method can explore resistivity down to ten or even a hundred kilometres, which makes it the EM method which has the most exploration depth of all the EM methods, and is practically the only method for studying resistivity deeper than at a few kilometres. The depth of penetration of electromagnetic fields within the earth depends on the period and the earth's conductivity structure. The propagation of EM fields is described by the following set of relationships, called the Maxwell's equation which holds true for all frequencies:

Faraday'slaw $$\boldsymbol{\nabla} \times \boldsymbol{E} = -\mu \frac{\partial \boldsymbol{H}}{\partial t} \quad (12)$$

Ampéré's law $$\boldsymbol{\nabla} \times \mathbf{H} = \mathbf{j} + \varepsilon \frac{\partial \mathbf{E}}{\partial t} \quad (13)$$

Gauss's law for the electric field $$div\mathbf{D} = \eta \quad (14)$$

Gauss's law for the magnetic field $$div\mathbf{B} = 0 \quad (15)$$

where **E** = Electrical field (V/m);
H = Magnetic intensity (A/m);
j = Electrical current intensity (A/m^2), and $\mathbf{j} = \sigma\mathbf{E}$;
μ = Magnetic permeability (H/m);
ε = Electric permittivity (F/m);
D = $\varepsilon\mathbf{E}$
B = $\mu\mathbf{H}$

2.4.1 Electromagnetic induction in a homogeneous earth

The ratio of electric to magnetic field intensity is a characteristic measure of electromagnetic properties, often called the characteristic impedance (Equations 16 and 17):

$$Z_{xy} = \frac{E_x}{H_y} = \frac{i\omega\mu}{k} \tag{16}$$

$$Z_{yx} = \frac{E_y}{H_x} = -\frac{i\omega\mu}{k} \tag{17}$$

where $Z_{xy}\ and\ Z_{yx}$ = Characteristic impedance in x and y directions;
$E_{x,y}$ = Electric field (V/m) in x, y direction;
$H_{x,y}$ = Magnetic intensity (A/m) in x, y direction;
ω = Angular frequency ($2\pi f$), where f is frequency (Hz);
k = $\sqrt{i\omega\mu(i\omega\varepsilon + \sigma)} \approx \sqrt{i\omega\mu\sigma}$ stands for the wave propagation constant;

and

$$Z_{xy} = \frac{E_x}{H_y} = \frac{i\omega\mu}{k} \approx \frac{i\omega\mu}{\sqrt{i\omega\sigma}} = \sqrt{i}\sqrt{\omega\rho\mu} = \sqrt{\omega\rho\mu}\cdot e^{i\pi/4} \tag{18}$$

$$Z_{yx} = \frac{E_y}{H_x} = -\frac{i\omega\mu}{k} = -Z_{xy} \tag{19}$$

The phase angle, θ, by which H_y lags E_x is $\pi/4$, is explained in Figure 11. If the earth is homogeneous and isotropic, then the true resistivity of the earth is related to the characteristic impedance through the following relationship (e.g. Hermance, 1973):

$$\rho = \frac{1}{\omega\mu}\left|Z_{xy}\right|^2 = \frac{1}{\omega\mu}\left|Z_{yx}\right|^2 \tag{20}$$

For a non-homogenous earth, the apparent resistivity *(ρ_a)* can be defined as if the earth were homogeneous using this same formula. In practical units for a homogeneous earth, the resistivity, ρ, in the above equation can be written as:

$$\rho_a = 0.2T|Z|^2 = 0.2T\left|\frac{E_x}{B_y}\right|^2 \tag{21}$$

For non-homogeneous earth, the apparent resistivity (ρ_a) and phase (θ_a) are functions of frequency and are defined as follows:

$$\rho_a = 0.2T|Z|^2 \text{ and } \theta = \arg(Z) \neq 45° \tag{22}$$

2.4.2 The impedance tensors

1D impedance tensor
For a 1D layered earth, the conductivity σ (or resistivity $\rho = 1/\sigma$) changes only with depth. In this case, the impedance tensor, $\boldsymbol{Z}$, may be written as:

$$Z_{1D} = \begin{bmatrix} 0 & Z_{xy} \\ -Z_{xy} & 0 \end{bmatrix} \tag{23}$$

For a layered earth, the apparent resistivity, ρ_{app}, is defined as:

$$\rho_{app}(\omega) = \frac{1}{\omega\mu_0}\left|Z_{xy}(\omega)\right| \tag{24}$$

The phase angle of the impedance is defined as:

$$\Phi(\omega) = \arctan\left(\frac{\Im(Z_{xy}(\omega))}{\Re(Z_{xy}(\omega))}\right) \tag{25}$$

Both the apparent resistivity in Equation 24 and the phase in Equation 25 depend on the angular frequency, $\omega = 2\pi f$ where f is the frequency.

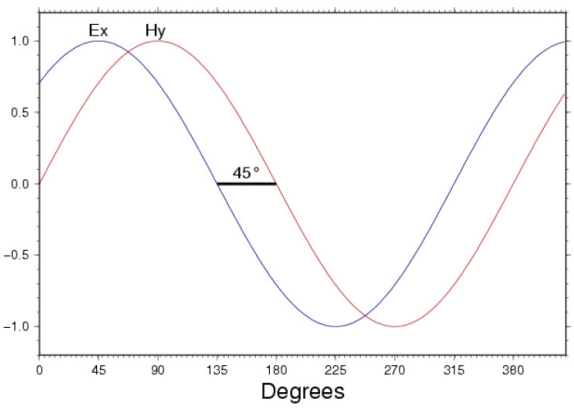

FIGURE 11: Homogeneous half-space response of the electric and magnetic fields describing the 45° phase difference of the **E** and **H** fields

2D impedance tensor

For a 2D earth, the conductivity, σ, changes with depth and in one horizontal direction. The other horizontal direction has no variation in conductivity and is commonly known as the electromagnetic or electrical strike direction.

The electrical strike direction gives information about the 2D resistivity structure, and in which direction the resistivity changes the least; often it is the same direction as the geological strike direction. The strike direction is found by minimizing the diagonal elements of the tensor Z_{xx} and Z_{yy}. However, there is a 90° ambiguity in the geoelectric strike. Measuring H_z and calculating the Tipper strike reveals this ambiguity. The strike is a function of frequency and is, therefore, different for different depths.

In Berdichevsky and Dmitriev (2002), it is shown by decomposing the ***E*** and ***H*** into normal and anomalous field components, that in a general 2D earth, the impedance tensor becomes:

$$Z_{2D} = \begin{bmatrix} Z_d & Z_{xy} \\ Z_{yx} & -Z_d \end{bmatrix} \tag{26}$$

Here, neither of the horizontal axes is aligned along the electromagnetic strike. In the impedance tensor, the diagonal elements $Z_{xx} = -Z_{yy} = Z_d$ are equal in amplitude but opposite in signs. The off diagonal elements Z_{xy} and Z_{yx} are independent values. However, if the impedance tensor is rotated such that the x direction is parallel and the y direction is perpendicular to the electromagnetic strike direction, the Z_{2D} impedance tensor simplifies to:

$$Z_{2D} = \begin{bmatrix} 0 & Z_{xy} \\ Z_{yx} & 0 \end{bmatrix} \tag{27}$$

The modes of the impedance tensor can be analysed independently. Transverse Electric (TE) mode or **E**-polarization is when the electric field is parallel to the electromagnetic strike and Transverse Magnetic (TM) mode or **B**-polarization is when the magnetic field is parallel to the electromagnetic strike. In Equation 27, the TE mode is $Z_{TE} = Z_{xy}$ and the TM mode is $Z_{TM} = Z_{yx}$. Apparent resistivity can be calculated for each of the modes such that:

$$\rho_{app_{TE}}(\omega) = \frac{1}{\omega\mu_0}|Z_{TE}(\omega)|^2 \;\; and \;\; \rho_{app_{TM}}(\omega) = \frac{1}{\omega\mu_0}|Z_{TM}(\omega)|^2 \tag{28}$$

And similarly, the phase angle:

$$\Phi_{\mathrm{TE}}(\omega) = \arctan\left(\frac{\Im(Z_{TE}(\omega))}{\Re(Z_{TE}(\omega))}\right) \; and \; \Phi_{\mathrm{TM}}(\omega) = \arctan\left(\frac{\Im(Z_{TM}(\omega))}{\Re(Z_{TM}(\omega))}\right) \tag{29}$$

3D impedance tensor

In a 3D earth model, the conductivity, σ (or resistivity ρ = 1/ σ) varies in all directions, σ (x, y, z). The impedance tensor takes the general form:

$$Z_{3D} = \begin{bmatrix} Z_{xx} & Z_{xy} \\ Z_{yx} & Z_{yy} \end{bmatrix} \tag{30}$$

All the elements in the impedance tensor in Equation 30 are non-zero elements. There is no direction where the diagonal elements of the impedance tensor vanish, so all the elements in the tensor need to be considered.

2.4.3 Skin depth

The skin depth, δ, is the depth where the electromagnetic field has been reduced to e^{-1} of its original value at the surface (Figure12). The propagation of the oscillating electromagnetic fields is time dependent, that is **H**, **E** ~ $e^{i\omega t}$ and it is a vertically incident plane wave. Therefore, skin depth is used as a scale length for the time-varying field, or an estimate of how deep such a wave penetrates into the earth and is given by:

$$\delta = \frac{1}{\mathrm{Real}(k)} = \frac{1}{\mathrm{Real}(i\omega\mu\sigma)} = \sqrt{\frac{2}{\omega\mu\sigma}} = \sqrt{\frac{2T\rho}{2\pi \cdot 4\pi \cdot 10^{-7}}} = \frac{10^3}{\pi} \cdot \sqrt{20/8} \cdot \sqrt{T\rho} \tag{31}$$

$$\delta \approx 500\sqrt{T\rho} \tag{32}$$

where δ = Skin depth (m);
T = Period (s); and
ρ = Resistivity (Ωm).

Figure 12 shows that low-frequency electromagnetic waves have a larger skin depth and thus penetrate deeper into the earth than high-frequency waves. High-frequency naturally occurring electromagnetic waves typically originate in worldwide lightning activity, and their small skin depth gives information about resistivity structures close to the surface. For lower frequencies, the electromagnetic wave penetrates deeper into the earth and senses resistivity at greater depths. These low-frequency electromagnetic waves originate in magnetospheric oscillations caused by the solar wind.

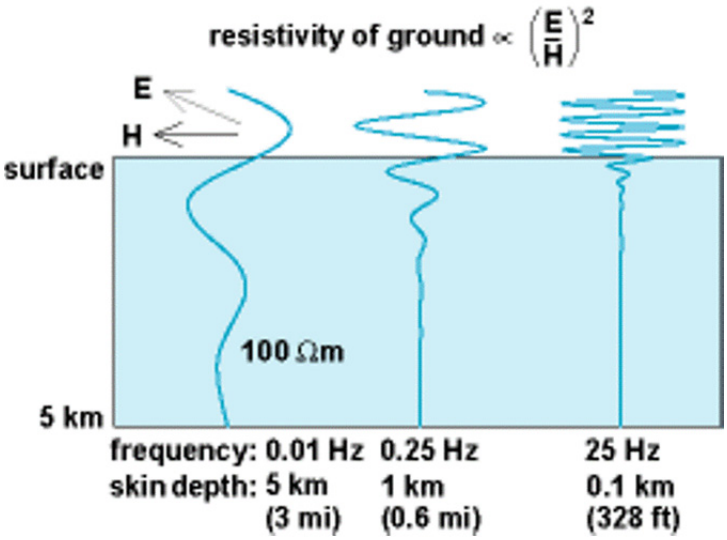

FIGURE 12: Difference in depth attenuation between low- and high-frequency electromagnetic waves (Unsworth, 2000)

3. TEM AND MT SURVEY IN THE AREA AROUND THE EYJAFJALLAJÖKULL GLACIER

3.1 Introduction

Eyjafjallajökull volcano is situated in a propagating rift outside the main zone of plate spreading in Iceland, at the southern termination of the eastern rift zone (Figure 13). The explosive eruption that began on 14th of April 2010 was the culmination of a long series of intermittent magmatic events observed over 18 years. This event caused an exceptional disruption to air traffic, closing airspace over much of Europe for days. The eruption was preceded by an effusive flank eruption of basalt from 20th March to 12th April.

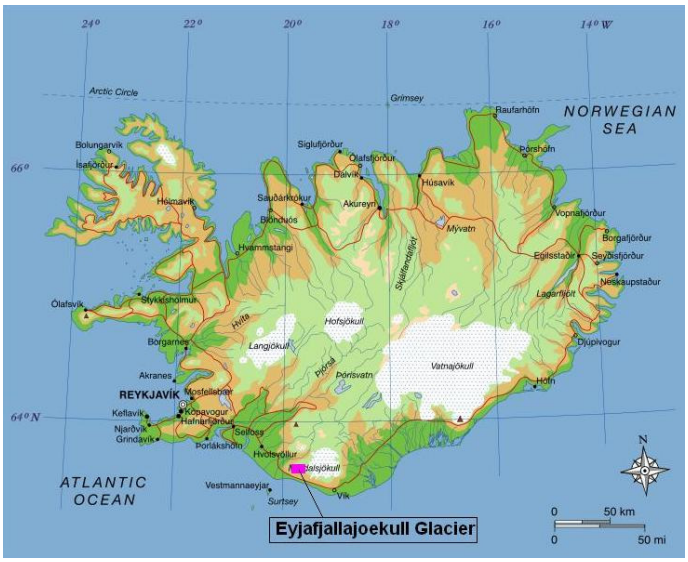

FIGURE 13: Map of Iceland with the geographical position of Eyjafjallajökull glacier

The transient electromagnetic (TEM) and the magnetotelluric (MT) methods were used to investigate the resistivity structure to a depth of several km beneath and around Eyjafjallajökull. As the presence of melt or partial melt enhances the bulk conductivity by one or more orders of magnitude, magma bodies will be imaged as low-resistive anomalies. The intention was to explore if and how these low-resistive structures are related to the recent volcanic activity below the glacier and to compare them with results from other methods and to similar investigations at other volcanic areas to identify similarities and disparities.

In July 2011, the Dublin Institute for Advanced Studies in Ireland (DIAS) in collaboration with the Iceland GeoSurvey (ISOR) carried out a pilot study deploying 26 MT/TEM sites in a 3D array distribution around Eyjafjallajökull (Miensopust et al., 2011).

3.2 TEM survey and equipment

The TEM survey was carried out by the field crew from Iceland GeoSurvey (ÍSOR). For the TEM resistivity survey, the Time Domain Electro Magnetics PROTEM digital receiver and a TEM-67 transmitter from Geonics Ltd. were used. For the purposes of this project, a total of 25 TEM soundings were carried out. For location, see Figure 14.

The sounding data were collected using a single turn transmitter wire loop of 200 × 200 m; one receiver loop was used. The transmitted current was usually in the range of 18-22 A, transmitted at a high frequency of 25 Hz, and a low frequency of 2.5 Hz. Repeated transients were stacked and stored in the computer memory of the receiver and later downloaded to a personal computer ready for further processing.

3.3 TEM data processing and interpretation

In TEM soundings a current is sent through a transmitter loop that excites the earth and the response is then measured using a receiver loop. The decay of the signal depends on the subsurface resistivity structure at the sounding site. The inversion problem is to determine the relevant physical parameters characterizing the system from the measured response in order to transform the data into more easily interpretable physical quantities. Forward modelling involves using the laws of physics to predict the

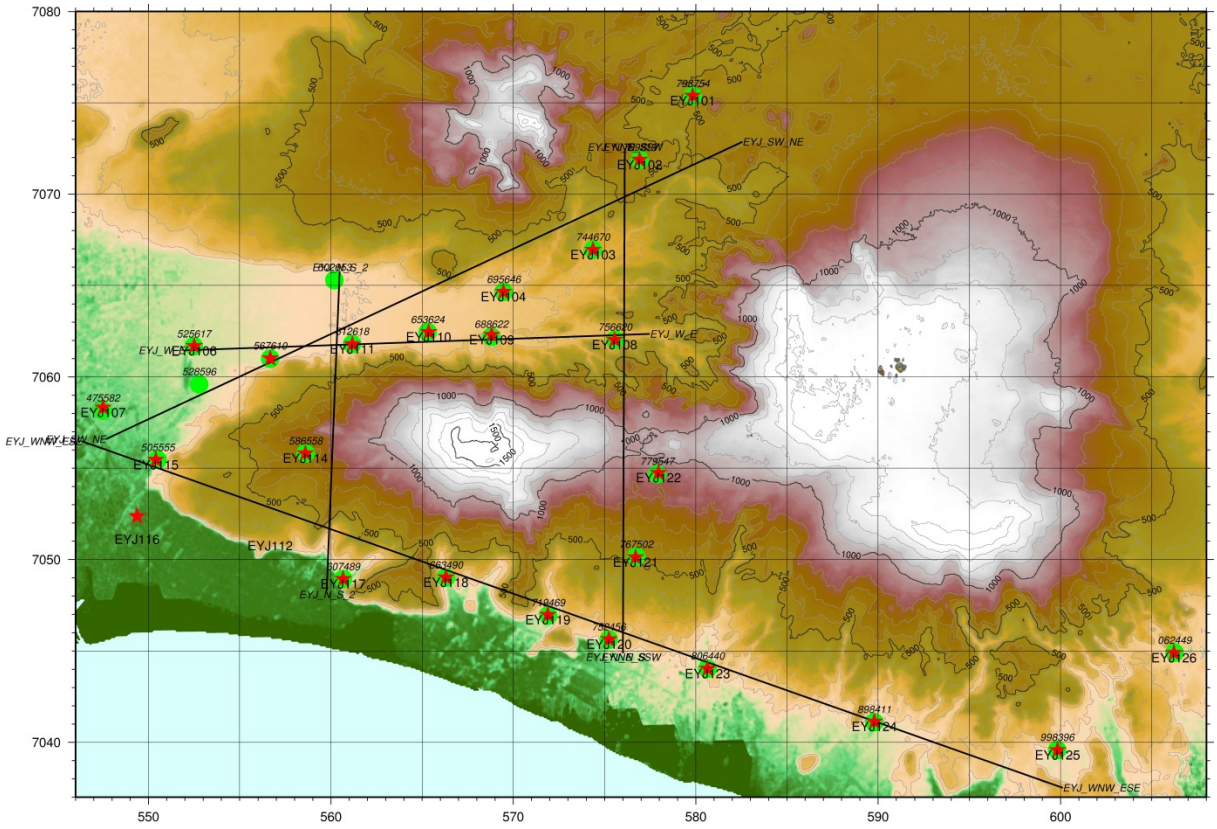

FIGURE 14: The TEM and MT sounding distribution and the locations of the cross-sections

observations from a model. A large set of models can be searched to find the one that fits the data (Figure 15).

The TemX program (Árnason, 2006a) was used to read raw data files downloaded from the receiver. It calculates averages and standard deviations for repeated transient voltage measurements and calculates late time apparent resistivity as a function of time. The program also offers the rejection of noisy readings through a graphical-user interface (GUI).

An interpretation program called TEMTD (Árnason, 2006b) was used to perform1D layered-earth inversion of the data. The program assumes that the source loop is a square loop and that the

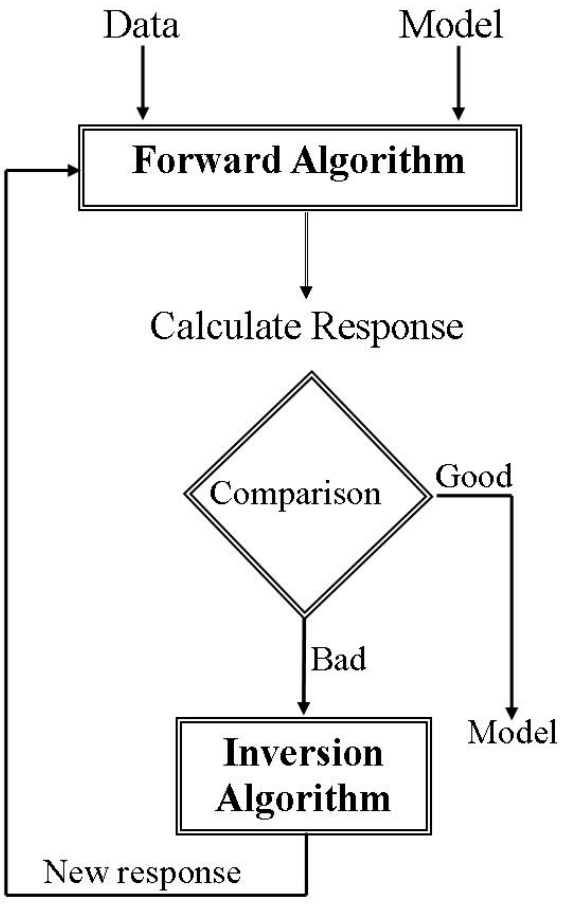

FIGURE 15: Diagram for the inversion procedure - the forward algorithm is used to calculate the response from a given model, which is compared with the measured data; if the comparison is good, the initial model is accepted. If the comparison is bad, the inversion algorithm is used to improve the model. The operation is continued until an acceptable fit is reached between the model response and the data

receiver coil/loop is at the centre of the source loop. The current wave form is assumed to be a half-duty bipolar semi-square wave with exponential current turn-on and linear current turn-off. The program also uses the GNUPLOT graphics program for graphical display during the inversion process.

The inversion algorithm used in the program is the nonlinear least-squares inversion of the Levenberg-Marquardt type (Árnason, 1989). The misfit function is the root-mean-square difference between measured and calculated values (chisq), weighted by the standard deviation of the measured values. The user is offered the option of choosing whether the program fits the measured voltage or the late time apparent resistivity values.

The program offers the possibility of keeping models smooth, both with respect to resistivity variations between layers (logarithm of conductivities) and layer thickness (logarithm of ratio of depth to top and bottom of layers). The damping can be done both on the first derivatives which counteract sharp steps in the model, and on the second derivatives which counteract oscillations in the model's values. The actual function that is minimised is not just the weighted root-mean-square misfit, *chisq*, but the potential:

$$Pot = chisq + \alpha * DS1 + \beta * DS2 + \gamma * DD1 + \delta * DD2 \qquad (33)$$

where *DS1* & *DS2* = First and second order derivatives of log-conductivities in the layered model;
DD1 & *DD2* = First and second order derivatives of logarithms of the ratios of layer depths;
α, β, γ & δ = Coefficients that are the relative contributions of the different damping terms.

The program is also used to perform minimum structure (Occam) inversion; in this case the layer thicknesses are kept fixed, equally spaced on a log scale, and the conductivity distribution is forced to be smooth by adjusting α and β in Equation 33. Figure 16 gives an example of the result after inversion of a TEM sounding. The TEM profiles of the 23 soundings used and their Occam inversion are given in Appendix I (Barkaoui, 2011).

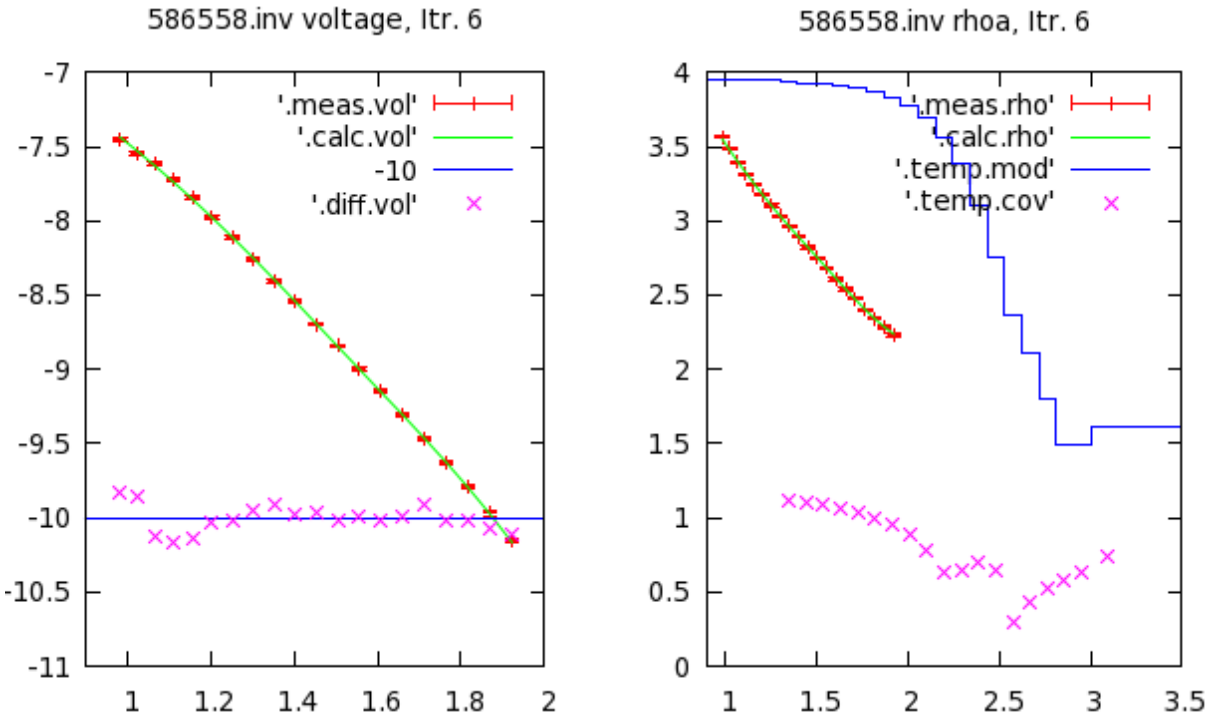

FIGURE 16: Inversion of TEM data

3.4 MT survey and equipment

The MT data were collected in collaboration with Iceland GeoSurvey (ÍSOR) and the Dublin Institute for Advanced Studies in Ireland (DIAS) within the same area where TEM sounding data were collected (Figure 14). A 5-channel MT data acquisition system (MTU-5A) from Phoenix Geophysics Canada was used. The instrumentation consisted of a data recorder, induction coils, non-polarizing electrodes, a Global Positioning System (GPS), a 12 V battery, flash memory for data recording, and telluric and magnetic cables.

The layout is made such that the electric dipoles are aligned in magnetic North-South and East-West, respectively, with corresponding magnetic channels in orthogonal directions; the third channel is vertical in the ground. Before data acquisition, a start-up file is prepared with parameters like gains, filters, time for data acquisition and calibrations for both equipment and the coils; this file is stored on a flash disk in the equipment.

The ground contact resistance is generally measured to gauge the electrode coupling to the ground to minimize the effect of self potential from the electric dipoles; an anti-aliasing filter is used, with a corner frequency of 0.005 Hz. The electric field was measured by lead chloride porous pots and the magnetic sensors were buried ~30 cm below the surface to minimize the wind and temperature effect.

MT data from each site were acquired for about 40 hrs., giving a frequency range of 320 Hz and often up to a period of few thousand seconds, which generally ensured investigation depths down to several tens of km. The penetration depth of the electromagnetic wave depends on the frequency where low-frequency waves have greater depth of penetration than high-frequency waves. During data acquisition, one 5-component MT station was installed far away from the survey area and maintained as a remote reference station which was later used during data processing to reduce the effect of local cultural noise. This is based on the fact that a magnetic signal tends to be the same over a large area and that local disturbances at the local station may not be recorded at the remote station, i.e. the noise part of the signal is not coherent at the two sites. During robust processing, estimates of magnetotelluric and geomagnetic response functions are determined using the coherency and expected uniformity of the magnetic source field as quality criteria. All the stations were time synchronized via signals from Global Positioning System (GPS) satellites so that time-series data from the remote reference station was processed in combination with data acquired at the same time from the other stations to reduce the effects of local noise and improve the quality of the survey results. A total of 26 MT soundings were considered, but only 24 were used and processed in this report.

3.5 MT data processing and interpretation

Time-series data downloaded from the MT equipment were processed by the SSMT2000 program, provided by the equipment manufacturer, Phoenix Geophysics of Canada. First the parameter file was edited to reflect the data acquisition setup and then the resulting time-series data were Fourier transformed to the frequency domain. The time series data were converted into the frequency domain by using a cascade decimation method. From the Fourier transform band, averaged cross and auto-powers were calculated using the robust processing method. The cross-powers were then graphically edited by the MTEditor program to remove the noisy data points and evaluate "smooth" curves for both phase and apparent resistivity (Figure 17). The final cross- and auto powers, as well as all relevant MT parameters calculated from them (impedances, apparent resistivity, phase coherences, strike directions etc.) were stored in industry-standard file formats (EDI files).
Figure 17 shows the following:

a) Apparent resistivity for both main modes (ρ_{xy} and ρ_{yx}) calculated in the measured directions i.e. x is magnetic north and y magnetic east. Black circles denote the apparent resistivity derived from the rotationally invariant determinant of the impedance tensor.

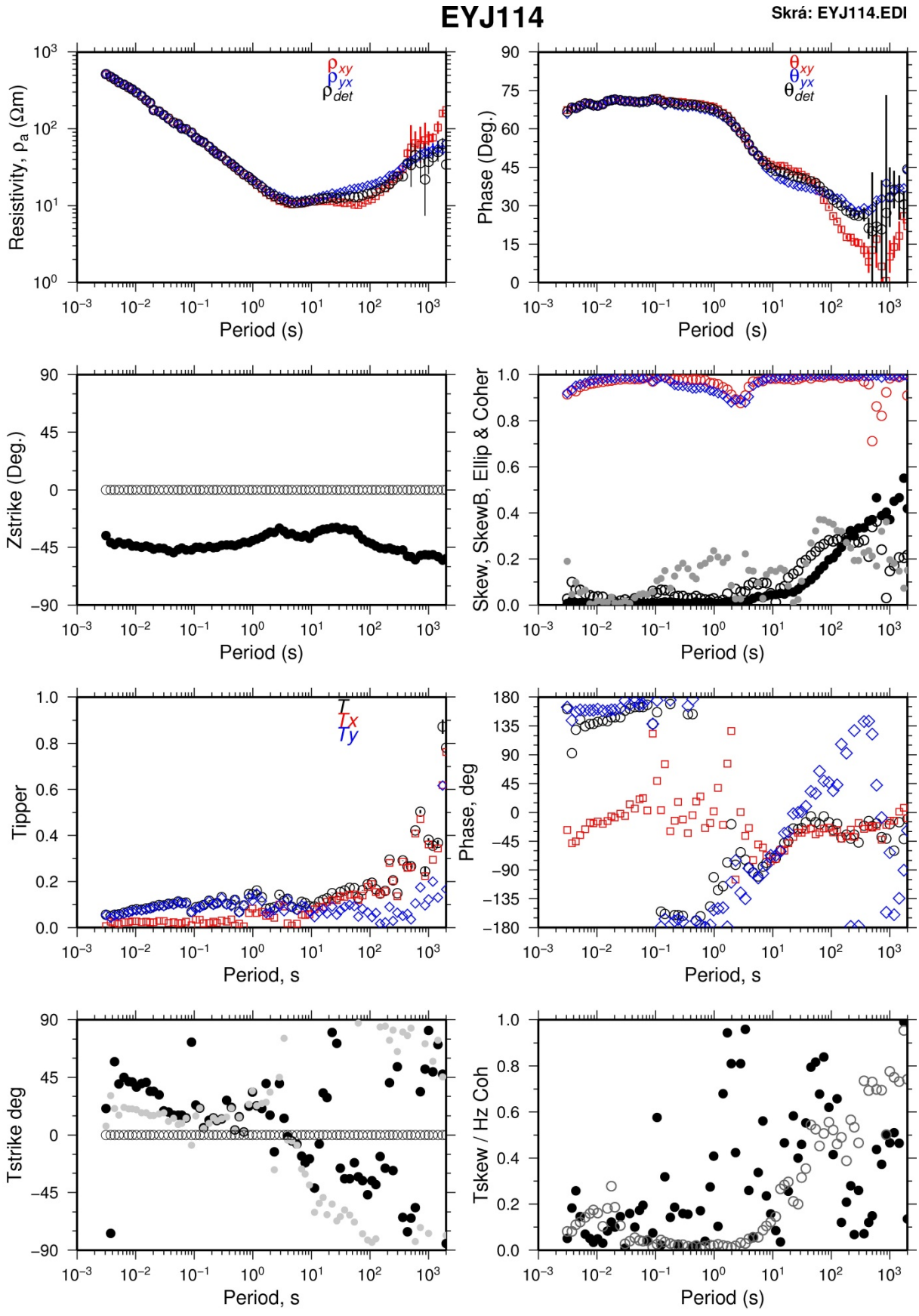

FIGURE 17: Results from MT data processing

b) Apparent phase ($\theta_{xy}$and θ_{yx}) calculated in the measured directions. Black circles denote the apparent phase derived from the rotationally invariant determinant of impedance tensor.
c) Zstrike or the Swift angle gives the electrical strike (the horizontal rotation which maximizes $|Z_{xy} + Z_{yx}|$ for each frequency and is shown by filled circles. The direction used for calculating the apparent resistivity and phase is shown by unfilled circles. For two-dimensional electrical structures, a constant value of electrical strike would be observed.
d) Three-dimensional indicators:
   Skew = $\frac{|Z_{xx}+Z_{yy}|}{|Z_{xy}-Z_{yx}|}$. Swift skew is shown by filled circles. It is rotationally invariant and should be zero for 1D and 2D earth.

   SkewB = $\frac{\sqrt{|\mathrm{Im}(Z_{xx}Z_{yy}^{*}+Z_{xx}Z_{yy}^{*})|}}{|Z_{xy}-Z_{yx}|}$ or Bahr skew is shown by unfilled circles. It is rotationally invariant and should be close to zero for both 1D and 2D earth.

   Ellip = $\left|\frac{Z'_{xx}-Z'_{yy}}{Z'_{xy}+Z'_{yx}}\right|$or ellipticity is shown by gray circles. It is calculated in the principle rotational coordinates and gives the axis rotation of the electrical field ellipse. A value of zero for both skew and ellipticity is a necessary and sufficient condition for two-dimensionality of the data.

   Red and blue colours on the *Skew, SkewB*, *Ellip* and *Coher* graph show the multiple coherencies of the electrical fields with respect to the horizontal magnetic fields in the measuring coordinates.
e) The Tipper which is calculated by using the *Z* component of H, H_z.

The results of the 24 MT soundings and the data processing are in Appendix II (Barkaoui, 2011).

3.5 Tipper strike direction

The electrical strike directions based on the Tipper are shown in Figure 18 for different periods. Zstrike has a 90° ambiguity, while the Tipper strike, which is based on the z component of the magnetic field, does not have this ambiguity. The z component was measured in most of the soundings. Figure 18 illustrates the Tipper strike direction for all periods (a); with an example for shallow depths, periods between 0.01 and 1 s (b), and in the last case, the Tipper strike direction at great depths, periods between 10 and 1000s (c). At this depth most of the soundings have the same Tipper direction due to the effects of the sea, which is a very good conductor.

3.6 The MT static shifts

The MT method suffers from the so called static shift problem. This phenomenon is caused by local resistivity inhomogeneities which disturb the electrical field. The main processes that cause static shift in MT measurements are voltage distortion, current distortion and the topographical distortion (Jiracek, 1990). The static shift is expressed by scaling of the apparent resistivity by an unknown factor (shifting on the log scale). This shift is independent of frequency, at least for those frequencies generally used in MT soundings (Jones, 1988). The static shifts can be a big problem in volcanic environments where resistivity variations close to the surface are often extreme. These parallel shifts in the apparent resistivity curve can lead to large errors in the inverted data. For instance, a shift down by S = 0.1 will, in interpretation, result in ten times too low resistivity values and about three times too small depths to resistivity boundaries (Árnason, 2008).

Several methods have been advanced as possible solutions for the static shift problem in MT. DeGroot-Hedlin (1991) and Ogawa and Ushida (1996) proposed the use of an inversion algorithm on

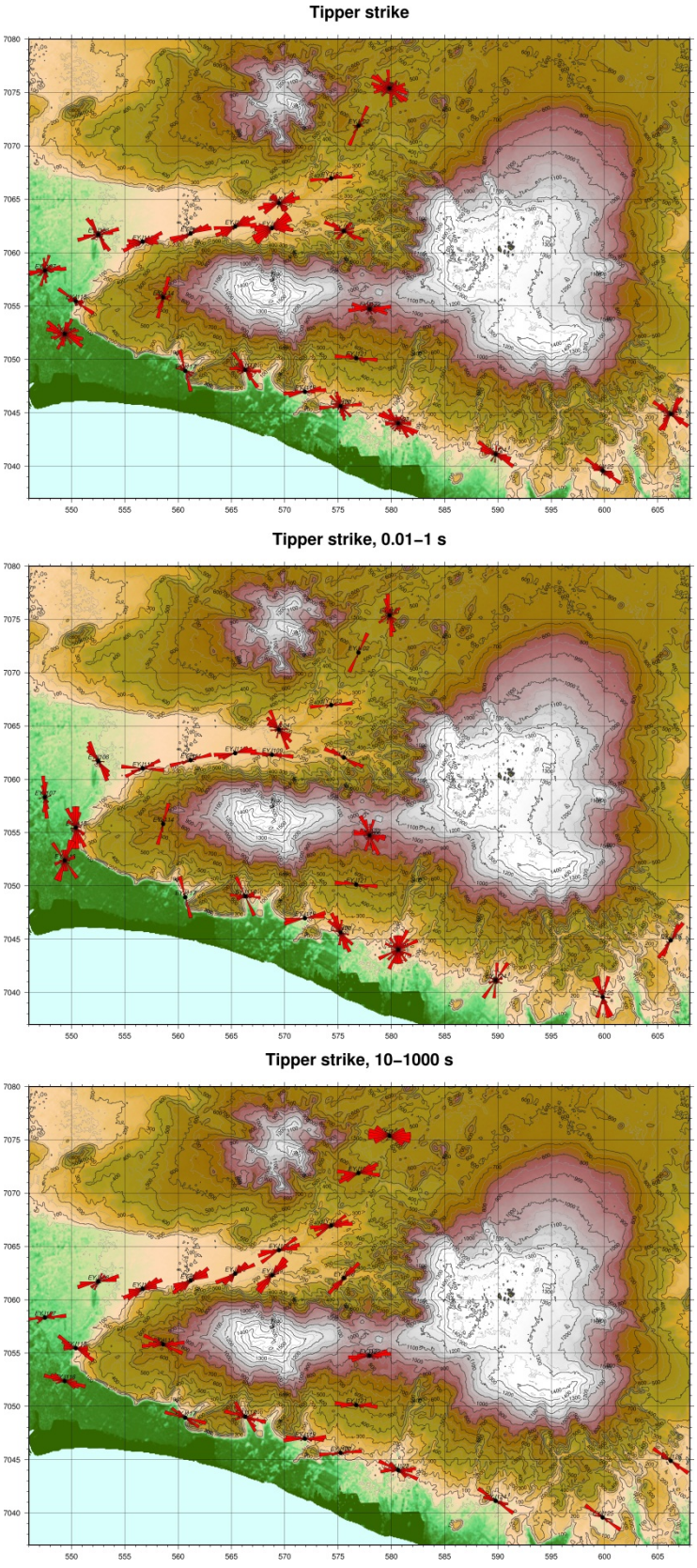

FIGURE 18: Rose diagram of the electrical strike based on the Tipper; a) For all periods; b) For periods between 0.01 and 1s; and c) For periods between10 and 1000 s

MT data themselves to correct for static shift; this assumes that the shift multipliers are random and that the product of the shift multipliers is close to one for many soundings. This may not necessarily be correct.

Another theory, and the one that has been used in this report, is the use of Central loop-induction TEM soundings to correct for static shift in MT data by jointly inverting both MT and TEM data. This is based on the fact that for TEM measurements at late time there are no distortions due to near surface inhomogeneities since they do not involve measuring the electrical field. This has been tested by model calculations (e.g. Sternberg et al., 1988) and shown to be a useful method for correcting for static shifts in MT soundings, at least for a 1D resistivity environment.

The TEM apparent resistivity used to estimate the shift parameter in the MT data does not necessarily agree with either of the principle apparent resistivities (*xy* or *yx*) . It may occur between them, below them or agree with either of them. It should also be noted that the phase is not affected by the static shift problem.

3.7 The MT static shift analysis of MT data in the Eyjafjallajökull area

Static shift analysis of the 24 MT soundings in the Eyjafjallajökull area was done using the TEMTD joint inversion code and inverting for the *rotational invariant determinant* apparent resistivity and phase data. The shift factors are in the range of 0.5-1.1. Most of the MT determinant apparent resistivity data were shifted down a shift factor around 0.8 (Figure 19).

Figure 20 shows the spatial distribution of the shift multipliers in the Eyjafjallajökull area. The map

shows that there are large areas where the MT apparent resistivity is consistently shifted downward.

In conclusion, it has been found that correction for static shift by use of controlled-source EM soundings and a joint inversion with MT data can be very effective in providing a more accurate picture of the resistivity structure of the earth.

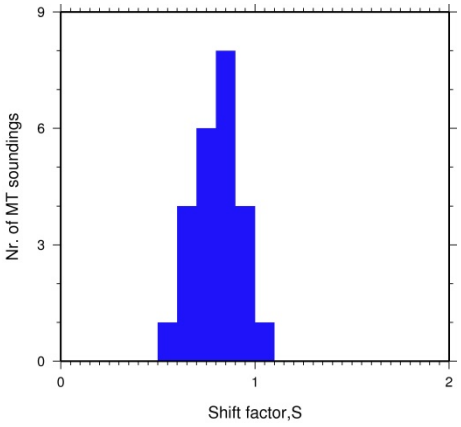

FIGURE 19: Histogram of shift factors applied to the MT apparent resistivity curves

3.8 Joint 1D inversion of the TEM and MT soundings

The TEMTD program does 1D inversion of TEM and MT data separately or jointly. In this study, the software was used to invert the MT apparent resistivity and phase derived from the rotationally invariant determinant of the MT tensor elements jointly with the TEM data. In the joint inversion, one additional parameter was inverted for, namely a static shift multiplier needed to fit both the TEM and MT data with the response of the same model. The program can do both standard layered inversion (inverting resistivity values and layer thicknesses) and Occam (minimum structure) inversion with exponentially increasing layer thicknesses with depth (see e.g. Constable et al., 1987). It offers a user specified damping of the first (sharp steps) and second order derivatives (oscillations) of model parameters (logarithm of resistivity and layer thicknesses) (Árnason, 2006b).

An example of a 1D joint inversion of MT and TEM data is shown in Figure 21. Red diamonds represent the TEM apparent resistivities transformed to a pseudo-MT curve. The blue squares represent the measured apparent resistivities and the blue circles pinpoint the apparent phase, both derived from the determinant of the MT impedance tensor. The light blue symbols to the left of the

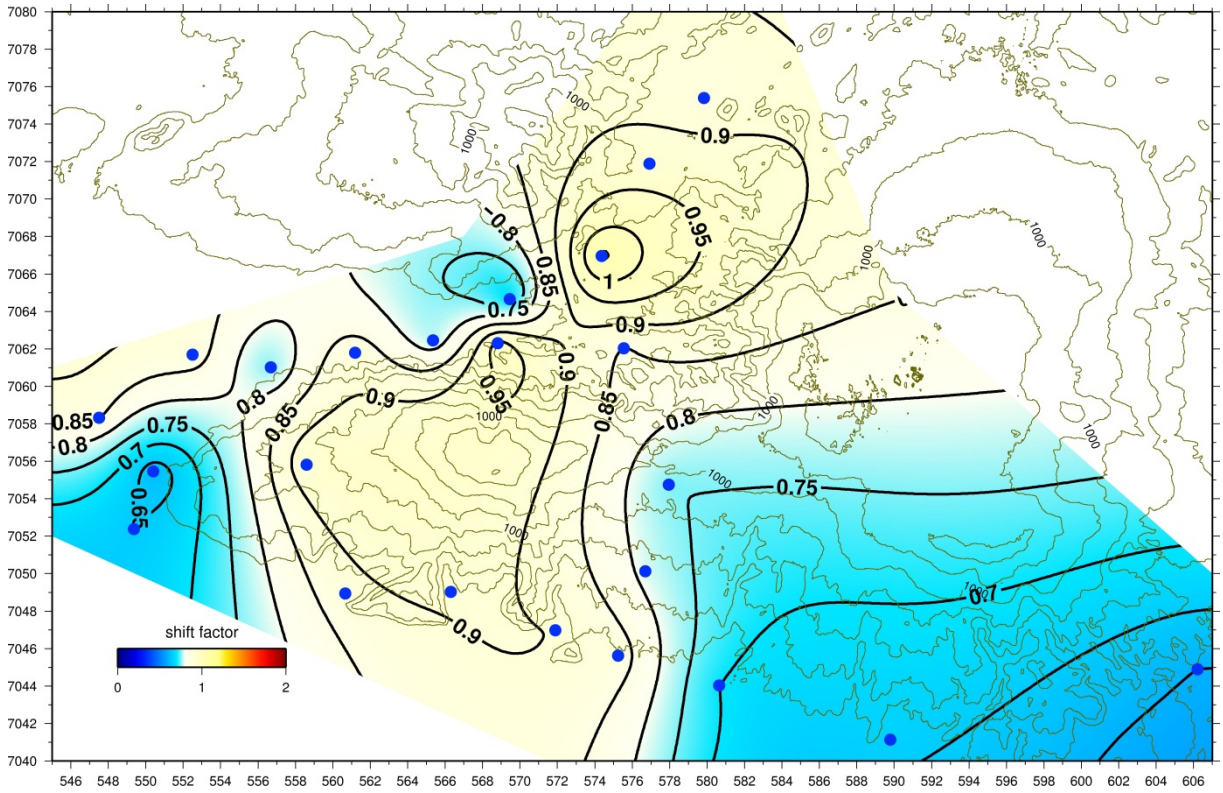

FIGURE 20: Static shift map of the Eyjafjallajökull area

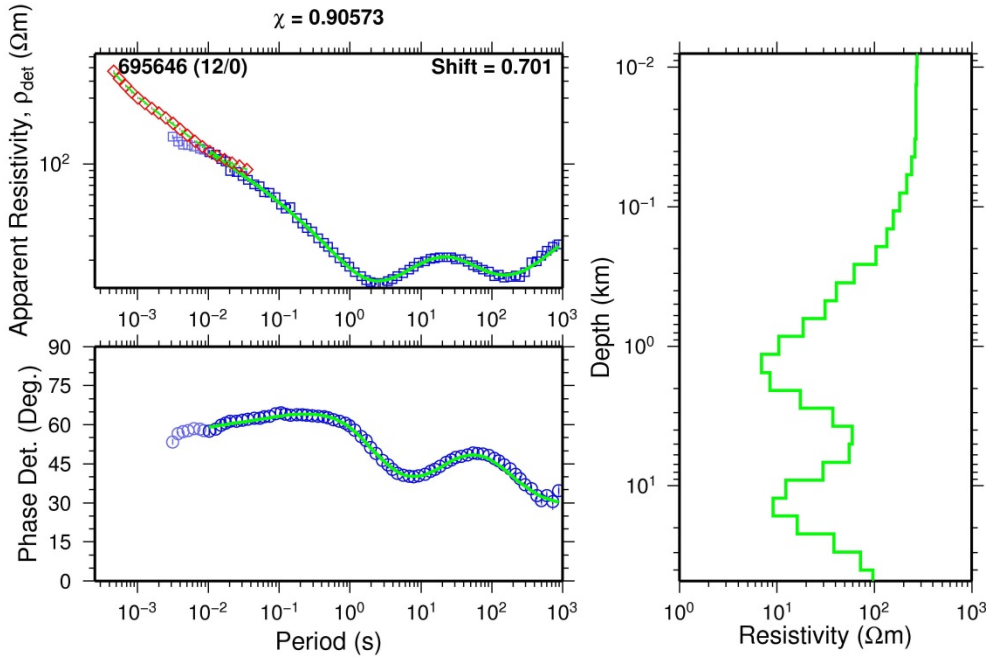

FIGURE 21: 1D joint inversion of a TEM and an MT sounding

green curve indicate data not used in the inversion. In the right panel are results of the 1D resistivity inversion model; in the left panel are the synthetic MT apparent resistivity and phase responses. The number in the upper left panel (695646) is the name of the TEM station. The numbers in parentheses (12/0) indicate that the two stations were 12 m apart with the same elevation, 0 m. The inversion results are shown by the following selected cross-sections and iso-resistivity maps. The 1-D joint inversion of all the MT and TEM profiles is given in Appendix III (Barkaoui, 2011).

Resistivity cross-sections were plotted from results obtained from 1D inversion by a program called TEMCROSS (Eysteinsson, 1998) developed at ÍSOR – Iceland GeoSurvey. The program calculates the best line between the selected sites on a profile and plots resistivity isolines based on the 1D model generated for each sounding. It is actually the logarithm of the resistivity that is contoured so that the colour scale is exponential, but the numbers at the contour lines are resistivity values.

Five vertical cross-sections were made through the survey area. Their location is shown on Figure 14. Cross-section N-S (Figure 22) shows a high-resistivity layer (> 100 Ωm), found close to the surface, reflecting fresh and unaltered rocks. Below the layer we can distinguish a conductive layer reflecting rocks rich of smectite and zeolite alteration minerals. At around 5 km depth, a resistive layer is detected reflecting a rich content of chlorite and epidote alteration minerals. Finally there is a conductive layer at around 15 km depth which is common in Iceland and has been interpreted as a possible indicator of high-temperature partial melt (see e.g. Björnsson et al., 2005). Figures 23-26 show similar results.

Iso-resistivity maps were made using the TEMRESD program, which generates iso-resistivity maps at different elevations from the 1D Occam models (Eysteinsson, 1998). The resistivity is contoured and coloured in a logarithmic scale. Five iso-resistivity maps were made at 1500, 5000, 10000, 12000 and 15000 m b.s.l. (see Figure 27-31). Generally, the maps show the conductive layers represented in the previously discussed cross-sections at the same level.

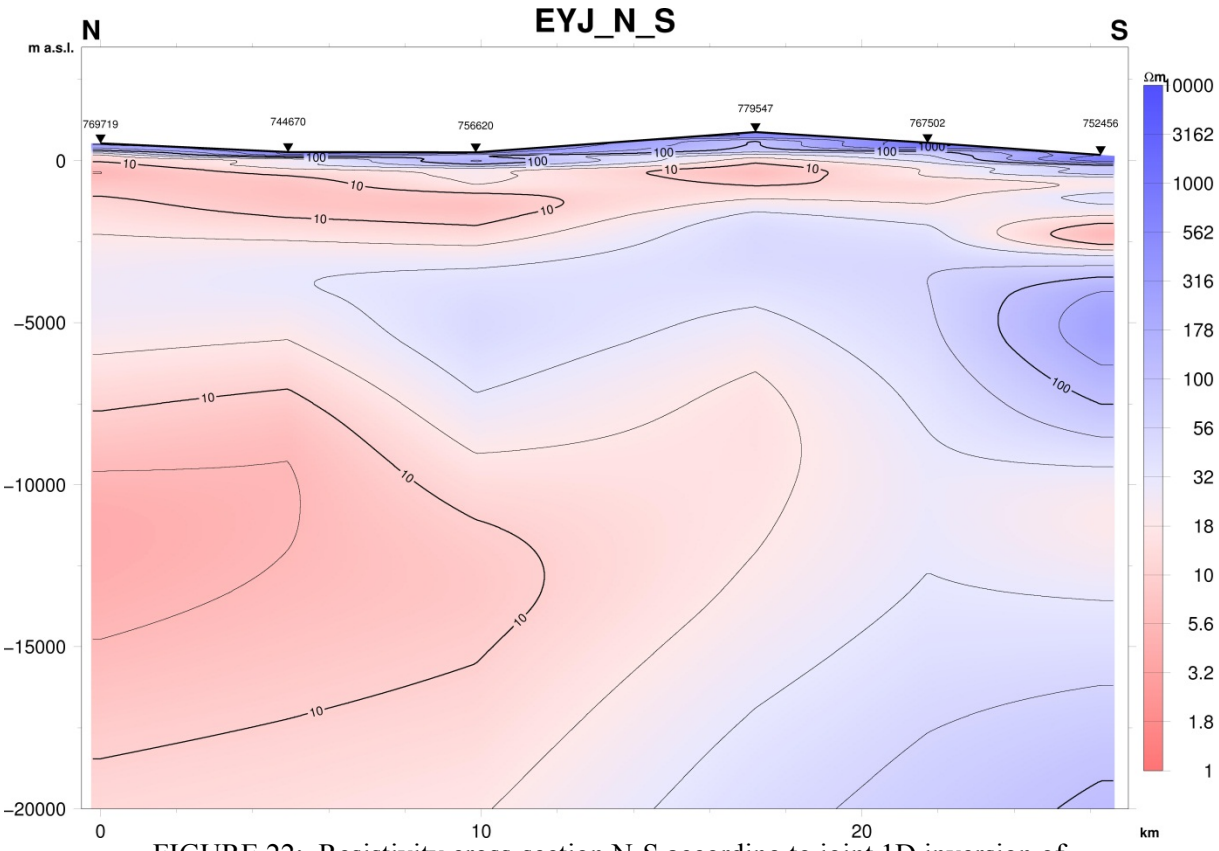

FIGURE 22: Resistivity cross-section N-S according to joint 1D inversion of TEM and MT data; the location is shown on Figure 14

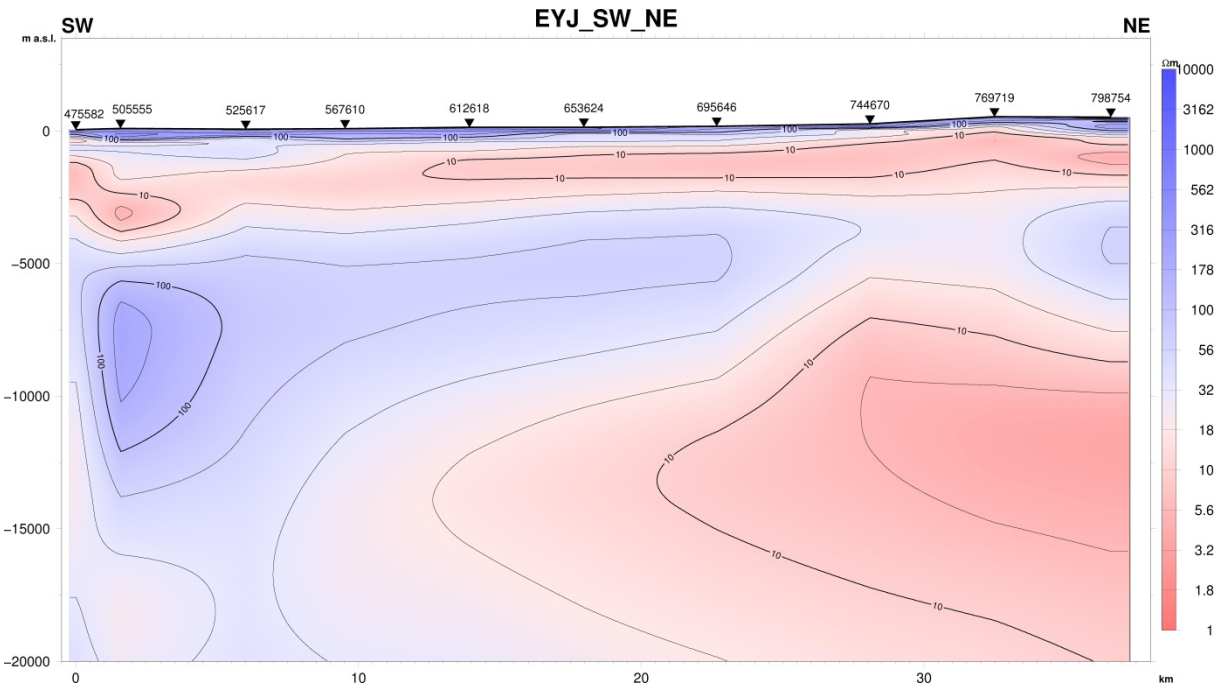

FIGURE 23: Resistivity cross-section SW-NE according to joint 1D inversion of TEM and MT data; the location is shown on Figure 14

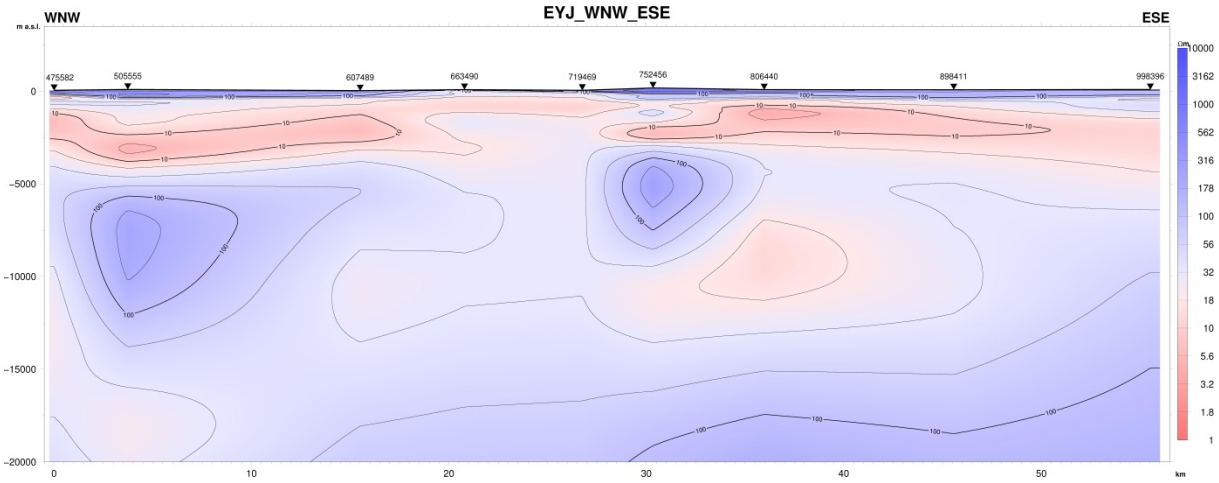

FIGURE 24: Resistivity cross-section WNW-ESE according to joint 1D inversion of TEM and MT data; the location is shown on Figure 14

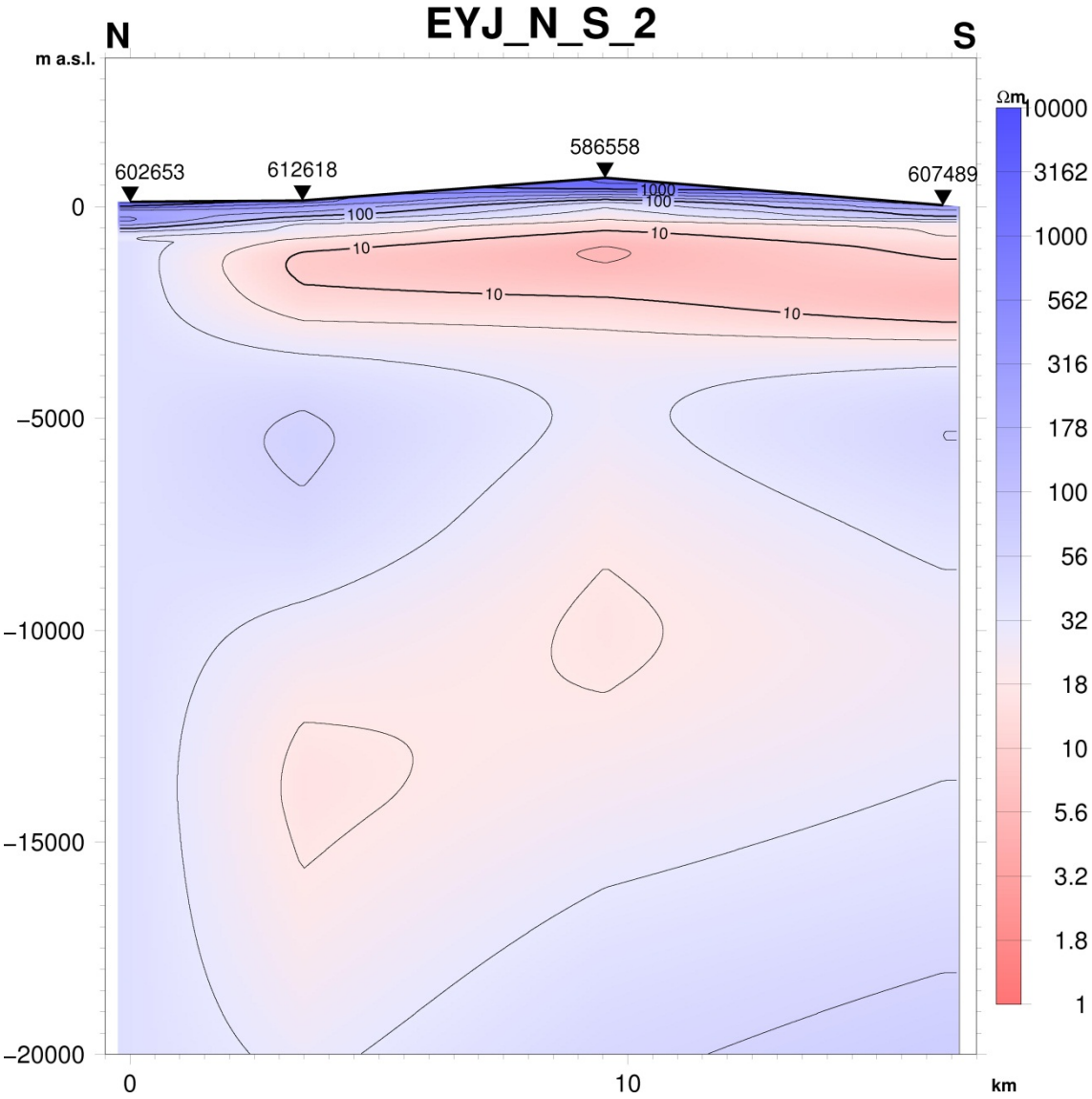

FIGURE 25: Resistivity cross-section N-S 2 according to joint 1D inversion of TEM and MT data; the location is shown on Figure 14

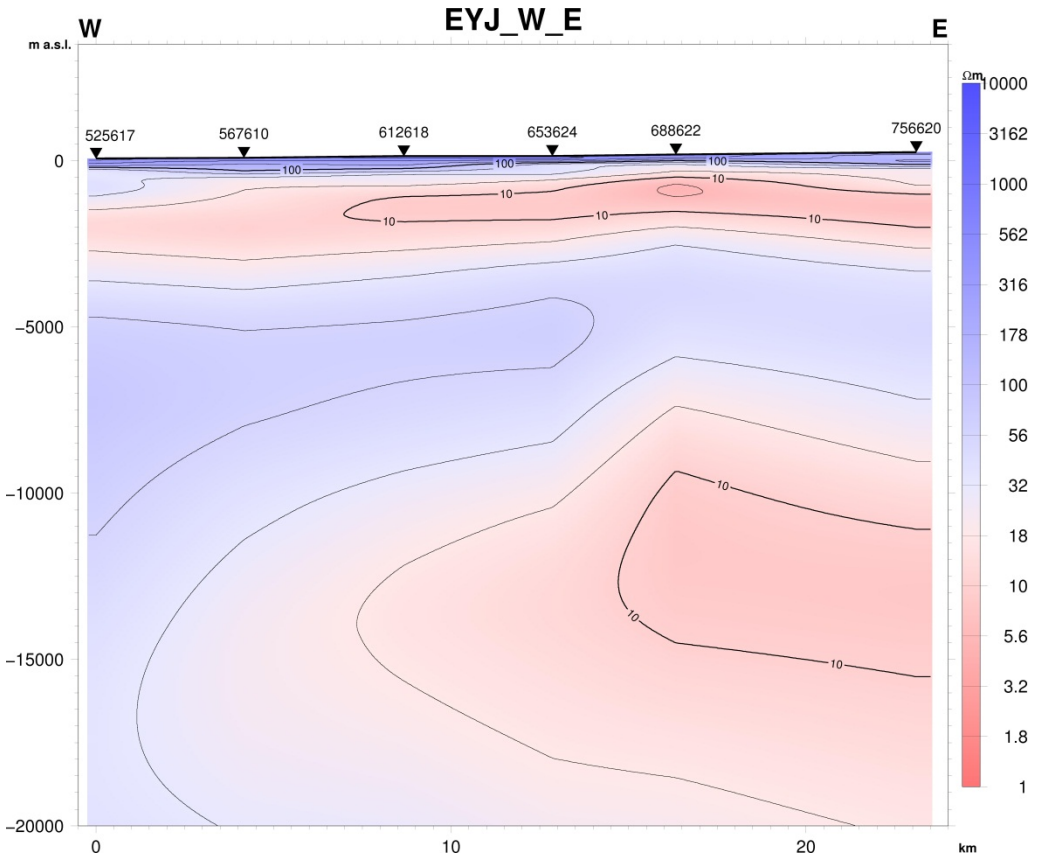

FIGURE 26: Resistivity cross-section W-E according to joint 1D inversion of TEM and MT data; the location is shown on Figure 14

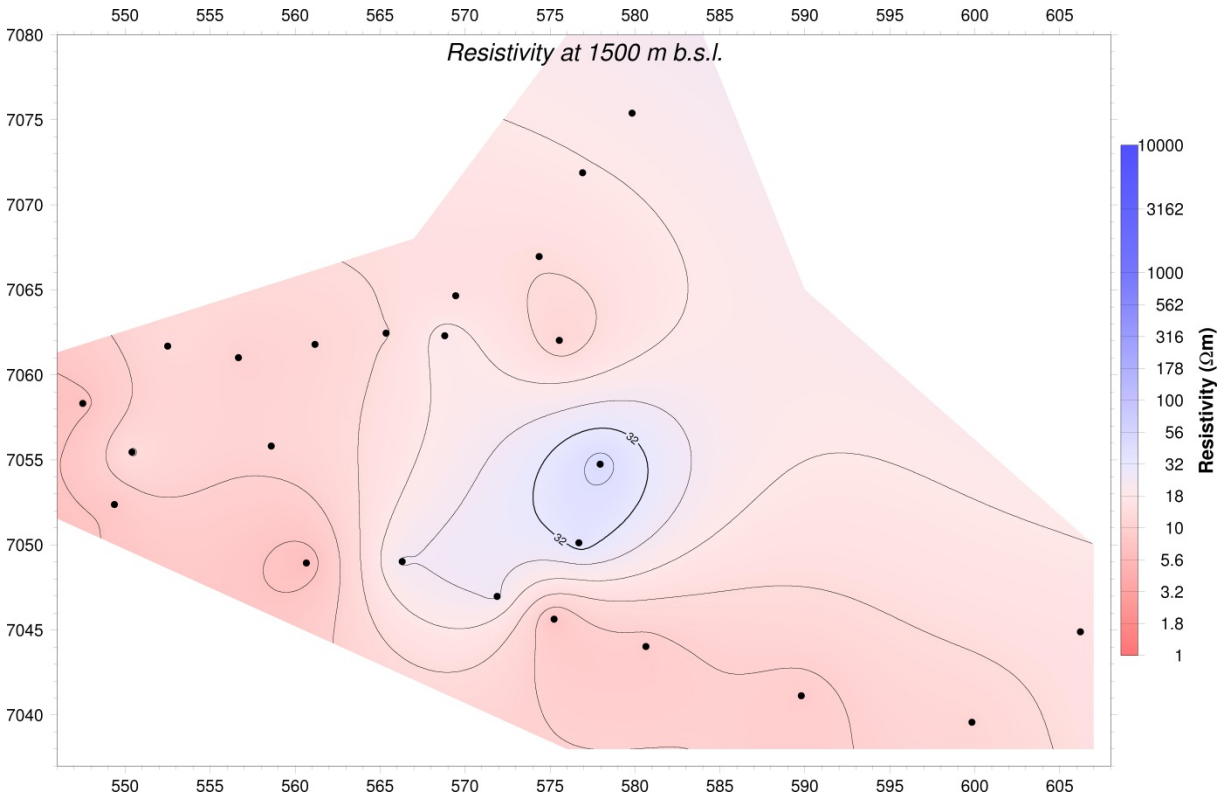

FIGURE 27: Iso-resistivity map at 1500 m b.s.l. based on joint 1D inversion of TEM and MT data

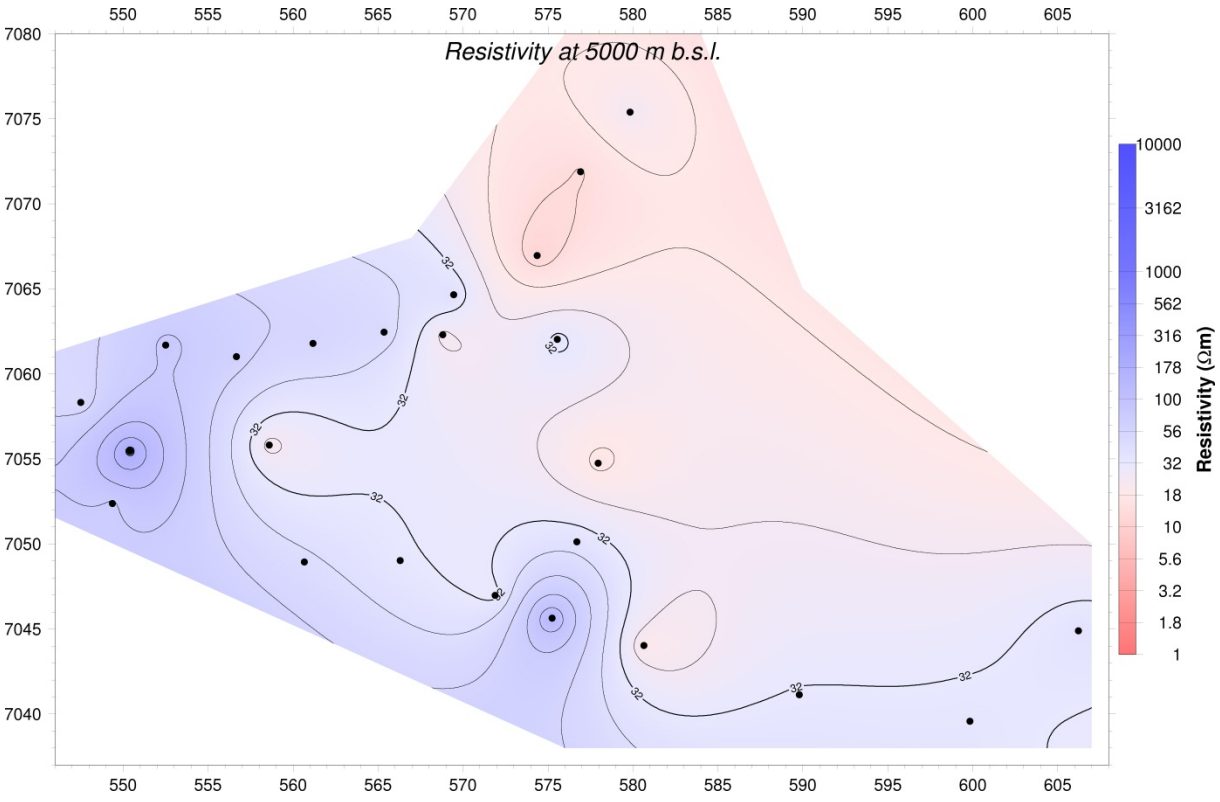

FIGURE 28: Iso-resistivity map at 5000 m b.s.l. based on joint 1D inversion of TEM and MT data

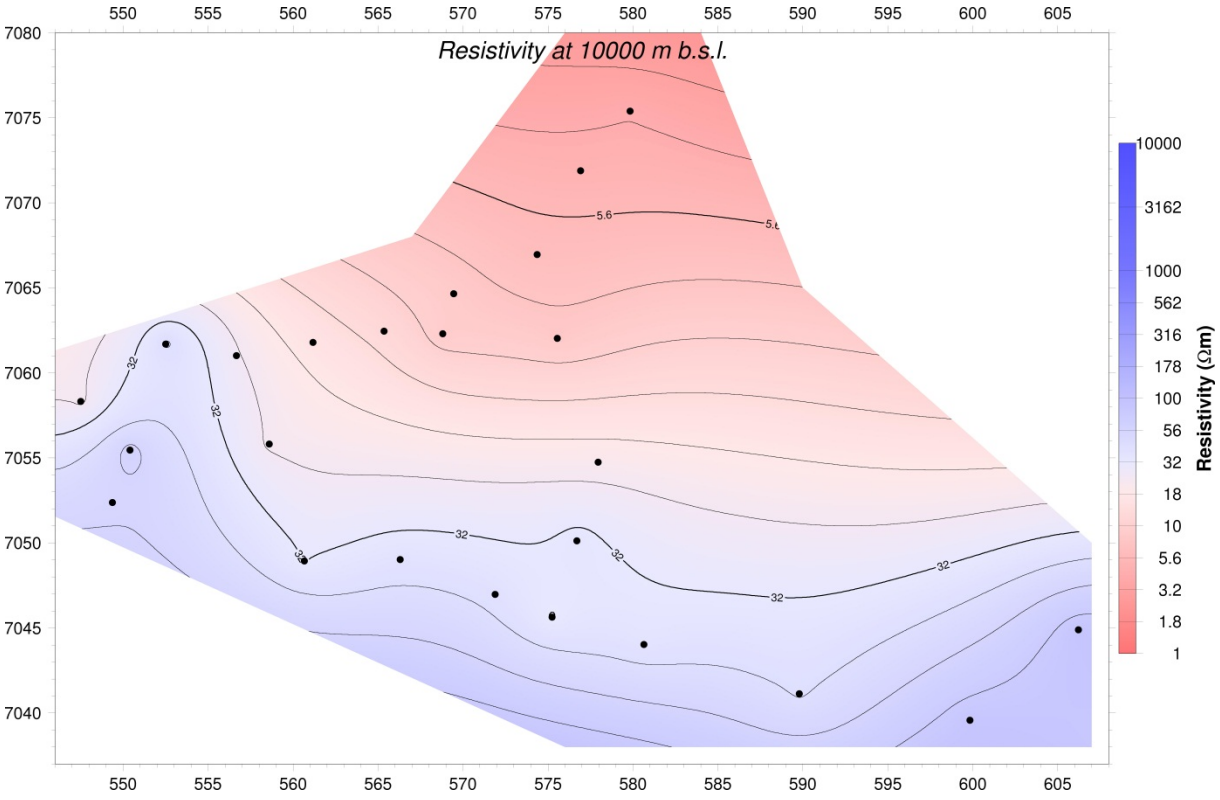

FIGURE 29: Iso-resistivity map at 10000 m b.s.l. based on joint 1D inversion of TEM and MT data

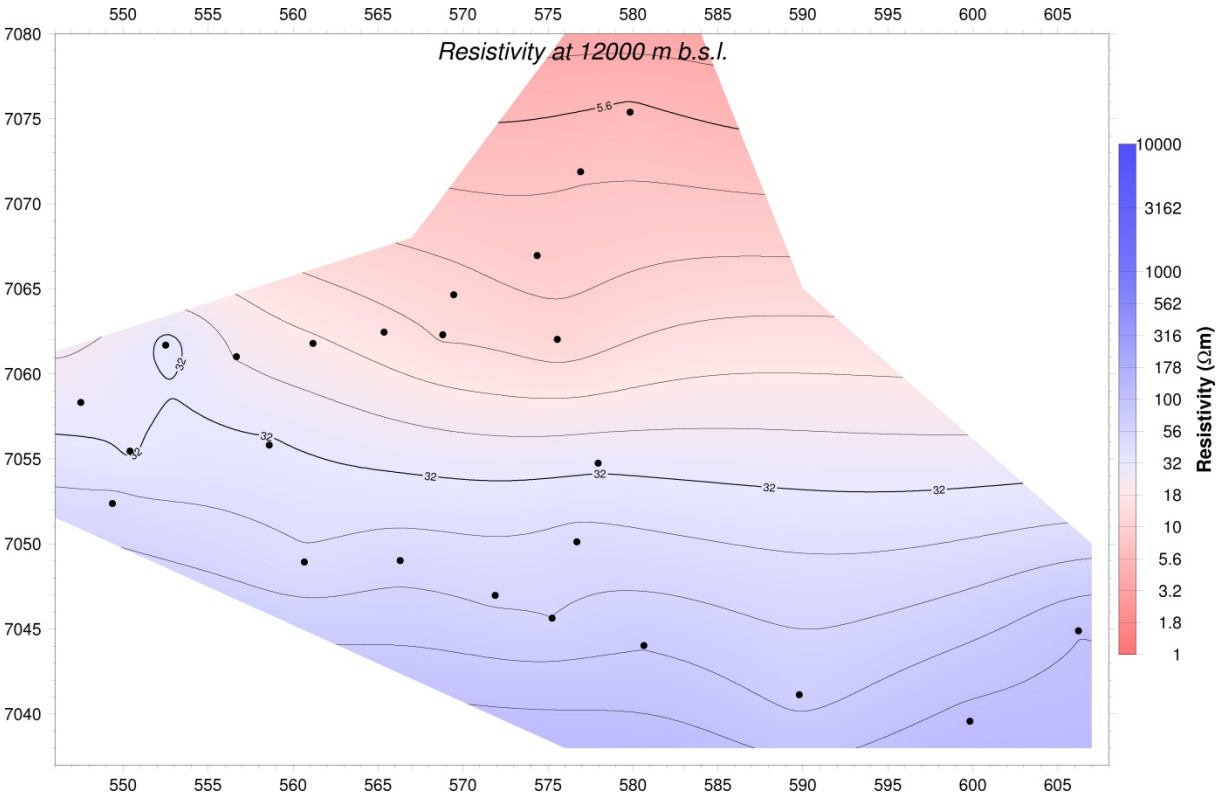

FIGURE 30: Iso-resistivity map at 12000 m b.s.l. based on joint 1D inversion of TEM and MT data

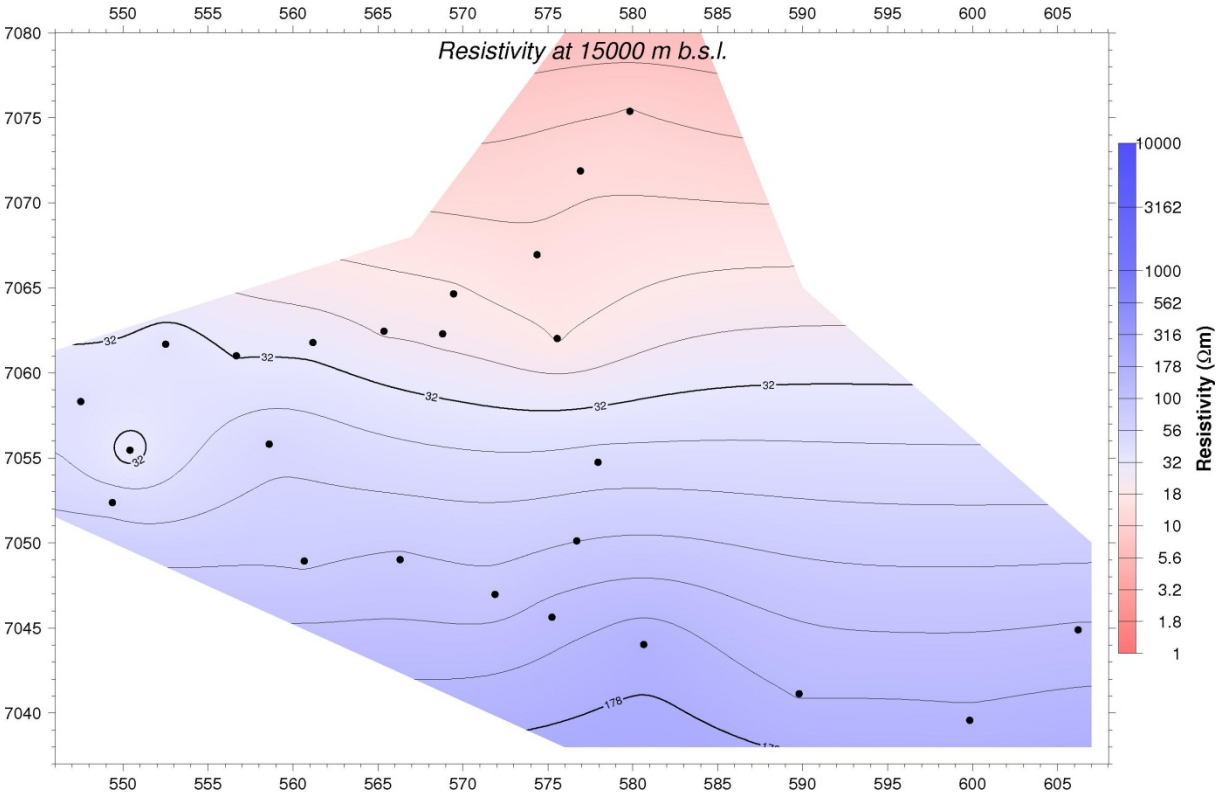

FIGURE 31: Iso-resistivity map at 15000 m b.s.l. based on joint 1D inversion of TEM and MT data

4. CONCLUSIONS

A total of 25 TEM and 26 MT soundings were performed in 2011 by the Dublin Institute for Advanced Studies (DIAS) and Iceland GeoSurvey (ISOR) in the Eyjafjallajökull area. The TEM-MT resistivity survey gives a good picture of the resistivity below the area around Eyjafjallajökull glacier.

Data inversion of the TEM/MT soundings was done using the 1D inversion program TEMTD. The MT data were jointly inverted with TEM data from the same location, to determine the best static shift parameter for the MT data. Static shift of these data are in the range from 0.5 to 1.1, the majority being around 0.8. The interpreted data are presented in the form of resistivity cross-sections and iso-resistivity maps as well as data curves and layered models.

Two conductive layers were detected, the first one at approximately 1-3 km depth, reflecting smectite and zeolite alteration minerals, and the second conductive layer at around 12 km depth, possibly indicative of high-temperature partial melt. This last layer is common in Iceland and conforms with many other MT observations across the country, especially in or near the volcanic zones (see e.g. Eysteinsson and Hermance, 1985).

ACKNOWLEDGEMENTS

I would like to express my gratitude to the UNU-GTP for awarding me this scholarship to participate in the six months training programme. Special thanks go to Dr. Ingvar Birgir Fridleifsson, the director, Mr. Lúdvík S. Georgsson, Ms. Thórhildur Ísberg, Mr. Ingimar G. Haraldsson and Mr. Markús A.G. Wilde, and all of UNU staff for their superb coordination of the training activities. Special thanks to my supervisors, Mr. Gylfi Páll Hersir and Mr. Knútur Árnason for their assistance and daily advice during the study time. I wish to give my thanks to Mr. Arnar Már Vilhjálmsson, Mr. Halldór Örvar Stefánsson, Mr. Egill Árni Gudnason and Mrs. Ragna Karlsdóttir from ÍSOR and Dr. Marion P. Miensopust, and Mr. Mark Muller at the Dublin Institute for Advanced Studies in Dublin.

I would like to acknowledge Prof. Yassine Zarhloule, my supervisor in the laboratory of Mineral Deposit, Hydrogeology and Environment, Prof. Mohamed Bouabedellah, director and Prof. Mimoun Boughriba, members of the same laboratory, for accepting my request to attend the six months programme in Iceland.

My deepest gratitude goes to my family for their moral and emotional support during these six months. To The Almighty God, who made all things possible, thank you.

REFERENCES

Archie, G.E., 1942: The electrical resistivity log as an aid in determining some reservoir characteristics. *Tran. AIME, 146,* 54-67.

Árnason, K., 1984: The effect of finite potential electrode separation on Schlumberger soundings. *54th Annual International SEG Meeting, Atlanta, Extended abstracts,* 129-132.

Árnason, K., 1989: Central-loop transient electromagnetic sounding over a horizontally layered earth. *Orkustofnun, Reykjavík, report OS-89032/JHD-06*, 129 pp.

Árnason, K., 2006a: *TemX. A graphically interactive program for processing central-loop TEM data, a short manual.* ÍSOR – Iceland GeoSurvey, Reykjavík, 10 pp.

Árnason, K., 2006b: *TEMTD. A program for 1D inversion of central-loop TEM and MT data, a short manual.*ÍSOR – Iceland GeoSurvey, Reykjavík, 16 pp.

Árnason, K., 2008: *The magneto-telluric static shift problem*. ÍSOR – Iceland GeoSurvey, Reykjavík, report ISOR-08088, 17 pp.

Árnason, K., Karlsdóttir, R., Eysteinsson, H., Flóvenz, Ó.G., and Gudlaugsson, S.Th., 2000: The resistivity structure of high-temperature geothermal systems in Iceland. *Proceedings of the World Geothermal Congress 2000, Kyushu-Tohoku, Japan*, 923-928.

Barkaoui, A., 2011: *Appendices to the report "Joint 1D inversion of TEM and MT resistivity data with an example from the area around the Eyjafjallajökull glacier, S-Iceland"*. UNU-GTP, Iceland, report 9 appendices, 44 pp.

Berdichevsky, M.N., and Dmitriev, V.I., 2002: *Magnetotellurics in the context of the theory of ill-posed problems.* Society of Exploration Geophysicists, USA, 215 pp.

Berktold, A., 1983: Electromagnetic studies in geothermal regions. *Geophysical Surveys, 6*, 173-200.

Björnsson, A., Eysteinsson, H., and Beblo, M., 2005: Crustal formation and magma genesis beneath Iceland: magnetotelluric constraints. In: Foulger, G.R., Natland, J.H., Presnall, D.C., Anderson, D.L. (eds), *Plates, plumes and paradigms*. Geological Society of America, Spec. Pap., 388, 665-686.

Cagniard, L., 1953: Basic theory of the magneto-telluric method of geophysical prospecting. *Geophysics, 18,* 605-635.

Chandrasekharam, D., and Bundschuh, J., 2008: *Low enthalpy geothermal resources for power generation*. Taylor and Francis Pub., UK, 169 pp.

Christensen, A., Auken, E., and Sorensen, K., 2006: The transient electromagnetic method. *Groundwater Geophysics, 71*, 179-225.

Constable, C.S., Parker, R.L., and Constable, C.G., 1987: Occam inversion: A practical algorithm for generating smooth models from electromagnetic sounding data. *Geophysics, 52*, 289-300.

Dakhnov, V.N., 1962: Geophysical well logging. Q. *Colorado Sch. Mines*, 57-2, 445 pp.

DeGroot-Hedlin, G., 1991: Removal of static shift in two dimensions by regularized inversion. *Geophysics, 56,* 2102-2106.

Eysteinsson, H., 1998: *TEMMAP and TEMCROSS plotting programs*. ÍSOR – Iceland GeoSurvey, Reykjavík, unpublished programs and manuals.

Eysteinsson, H., and Hermance, J.F., 1985: Magnetotelluric measurements across the eastern neovolcanic zone in south Iceland. *J. Geophys. Res, 90,* 10093–10103

Flóvenz, Ó.G., Georgsson, L.S., and Árnason, K., 1985: Resistivity structure of the upper crust in Iceland, *J. Geophys. Res., 90-B12*, 10,136-10,150.

Flóvenz, Ó.G., Spangenberg, E., Kulenkampff, J., Árnason, K., Karlsdóttir, R., and Huenges, E., 2005: The role of electrical conduction in geothermal exploration. *Proceedings of the World Geothermal Congress 2005, Antalya, Turkey*, CD, 9 pp.

Hermance, J.F., 1973: Processing of magnetotelluric data. *Earth and Planetary Interiors, 7*, 349 - 364, Netherlands.

Hersir, G.P., and Árnason, K., 2009: Resistivity of rocks. *Paper presented at the Short Course on Surface Exploration for Geothermal Resources, organized by UNU-GTP and LaGeo, Santa Tecla, El Salvador*, 8 pp.

Hersir, G.P., and Björnsson, A., 1991*: Geophysical exploration for geothermal resources. Principles and application.*UNU-GTP, Iceland, report 15, 94 pp.

Jiracek, G. R., 1990: Near-surface and topographic distortions in electromagnetic induction. *Surveys in Geophysics, 11,* 163-203.

Jones, A.G., 1988: Static shift of magnetotelluric data and its removal in a sedimentary basin environment. *Geophysics, 53-7,* 967-978.

Jones, A.G., Chave, A.D., Egbert, G., Auld B., and Bahr, K., 1989: A comparison of techniques for magnetotelluric response function estimation. *J. Geophys. Res., 94(B10)*, 14201-14213.

Keller, G.V., and Frischknecht, F.C., 1966: *Electrical methods in geophysical prospecting.* Pergamon Press Ltd., Oxford, 527 pp.

Miensopust, M.P., Jones, A.G., Hersir, G.P., and Vilhjálmsson, A.M., 2011: *Electromagnetic investigations of the resistivity structure around and beneath the Eyjafjallajökull volcano, Southern Iceland: preliminary results.* Poster presented at Schmucker-Weidelt Colloquium, 26th-30thseptember 2011.

Nabighian, M.N., and MacNae, J.C., 1988: TDEM prospecting methods. In: Nabighian, M.N. (ed.), *Electromagnetic methods in applied geophysics 1, theory*. Soc. Expl. Geophys., Tulsa, OK, 427-520.

Nabighian, M.N., and MacNae, J.C., 1991: Time domain electromagnetic prospecting methods. In: Nabighian, M.N. (ed.), *Electromagnetic methods in applied geophysics - application, part A, vol.2*. Soc. Expl. Geophys., Tulsa, OK, 427-509.

Ogawa, Y., and Ushida, T., 1996: A two-dimensional magnetotelluric inversion assuming Gaussian static shift. *Geophys. J. Int., 126*, 69-76.

Quist, A.S., and Marshall, W.L., 1968: Electrical conductances of aqueous sodium chloride solutions from 0 to 800°C and at pressures to 4000 bars. *J. Phys. Chem., 72*, 684-703.

Rosenkjær, G.K., 2011: *Electromagnetic methods in geothermal exploration. 1D and 3D inversion of TEM and MT data from a synthetic geothermal area and the Hengill geothermal area, SW Iceland.* University of Iceland, MSc thesis, 137 pp.

Sternberg, B.K., Washburne, J.C., and Pellerin, L., 1988: Correction for static shift in magnetotellurics using transient electromagnetic soundings. *Geophysics, 53*, 1459-1468.

Tikhonov, A.N., 1950: Determination of the electrical characteristics of the deeper strata of the earth's crust. *Dokl. Akad. Nauk, USSR, 7-2.*

Unsworth, M., 2000: Magnetotellurics. In: *McGraw-Hill 2000 Yearbook of Science and Technology.* McGraw-Hill, NY, 240-242.

Vozoff, K., 1991: The magnetotelluric method. In: Nabighian, M.N (ed), *Electromagnetic methods in applied geophysics, Vol. II*, 641-711.

Zhdanov, M.S., and Keller, G.V., 1994: *The geoelectric methods in geophysical exploration.* Elsevier, Amsterdam, 873 pp.